3D PERMEABILITY CHARACTERIZATION OF FIBROUS MEDIA

by

Kenneth Okonkwo

A thesis submitted to the Faculty of the University of Delaware in partial fulfillment of the requirements for the degree of Master of Science in Mechanical Engineering

Summer 2010

3D PERMEABILITY CHARACTERIZATION OF FIBROUS MEDIA

by

Kenneth Okonkwo

Approved: ____
Suresh G. Advani, Ph.D.
Professor in charge of thesis on behalf of the Advisory Committee

Approved: ____
Annette M. Karlsson, Ph.D.
Chair of the Department of Mechanical Engineering

Approved: ____
Michael J. Chajes, Ph.D.
Dean of the College of Engineering

Approved: ____
Debra Hess Norris, M.S.
Vice Provost for Graduate and Professional Education

ACKNOWLEDGMENTS

I would like to acknowledge the National Science Foundation (NSF) for supporting this work under the grant number 0856399.

I would like to give special thanks to Prof. Suresh G. Advani, who has been a very supportive advisor all along my master's program.

And also a big thanks to Dr. Pavel Simacek who helped me out in several ways whenever I had questions. I am also grateful to Paul, Justin, Chad and others in the laboratory who all made it possible for this program to become a reality.

Lastly but not the least I would say a big thank you to my wife, Sis. Tumi Okonkwo, for being there all the way.

TABLE OF CONTENTS

Appendix

LIST OF TABLES

LIST OF FIGURE

ABSTRACT

In Liquid Composite Molding (LCM) processes, a liquid resin is forced to flow through dry fibrous preform, usually fabrics, to impregnate it and create the composite part in net or near-net shape. The principal advantage of LCM processes is their capacity to produce high fiber volume fraction and high quality parts under low pressure at low cost. The main conditions for successful manufacturing are complete filling of the mold and perfect impregnation of the reinforcement material. If these conditions are not met the structural properties of the finished part are significantly impaired by defects like voids.

The mold filling depends on the permeability of the fibrous media. Permeability is an intrinsic property of fiber reinforcement, which includes all interactions between fibers and fluid and characterizes the ease of flow through the medium. The complete prediction of second-order permeability tensor is critical to understanding and prediction of flow in the resin transfer molding process of thick composites or where the flow process is three dimensional

In this thesis a new approach for characterizing the three dimensional permeability tensor of fabrics used as reinforcement in liquid injection molding processes from a single experiment is presented and validated. In this approach, a liquid is injected into a preform placed in a mold containing 192 electrical resistance flow sensors radially embedded in the top and the bottom platens of the mold. The proposed method uses an optimization routine in which the permeabilities in a 3D

flow simulation of the identical mold is updated continuously until the error between the simulation arrival times at all the 192 sensor locations and the experimental arrival time is minimum. The optimization routine systematically changes the values of the components of the permeability tensor using golden search method until the best match is obtained. The validation and sensitivity of this method is explored and it has been shown that this technique is promising for permeability characterization. The approach is shown to be valid for reinforcements with anisotropic and isotropic nature

The advantage of this approach is that it can be used to obtain permeability values from a single experiment; there is no need to scale the circular injection inlet, and it is not limited to principal permeability values. The sensors utilized are unobtrusive to the flow unlike say optic fibers embedded in the fabric that interfere with the flow of the test fluid. The electrical resistance sensors used in this approach are embedded in mold platens instead and which flush with the surface. The method can be used to help predict and understand resin flow behavior during liquid molding of advanced composite materials.

Chapter 1

INTRODUCTION

1.1 Permeability of Fibrous Materials in Liquid Composite Molding Processes

In Liquid Composite Molding (LCM) processes, a liquid resin is forced to flow through dry fibrous preform, usually fabrics, to impregnate it and create the composite part in net or near-net shape. The principal advantage of LCM processes is their capacity to produce high fiber volume fraction and high quality parts under low pressure at low cost. Resin Transfer Molding is one of the most widely used LCM process and is the focus of this study.

In a traditional RTM process; catalyzed thermosetting liquid resin is injected into an enclosed metal mold containing a previously positioned reinforcement preform. The preform is compacted to the specified fiber volume fraction when the matched metal mold is closed. The goal is to cover all the empty spaces between the fibers with the resin before the resin arrives at the vent at which the point injection is discontinued. As the resin was catalyzed it continues to cure in the mold. The part is demolded once most of the cross-linkage has occurred and the part is rigid. A schematic diagram of the process is shown in Figure 1.1.

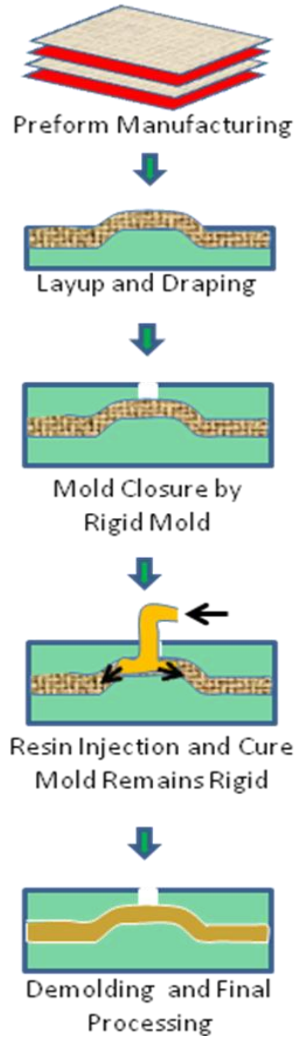

Figure 1. 1: Resin Transfer molding process (redrawn from [1])

In order to obtain good-quality products, the fibrous preform must be fully saturated with resin. Any dry spots within the part lead to reduced quality, costly repairs or outright rejection. Hence the positioning of resin injection inlet and air vents in the mold is a very important part of the process design. In recent years, flow simulation software is replacing the (expensive) trial-and-error way of optimizing the layout of molds and injection gates and vents [2]. However, to be able to predict the filling of the mold correctly, these simulation codes need a reliable input of geometric and material parameters such as mold geometry dimensions, fluid viscosity, reinforcement porosity, and reinforcement permeability. Hence the success of the simulation to predict how the resin impregnates the mold and the time it takes to do so depends to a great extent on the accuracy of the permeability data [3].

The concept of permeability originates from the established theory of transport phenomena in porous media and has been extensively applied in the modeling of casting defect formation [4]. Flow through porous media is governed by Darcy's law that relates the viscosity of the resin, the permeability of the preform, with the pressure gradient and the average velocity of the fluid as follows:

$$\overline{u} = -\frac{K}{\eta} \cdot \overline{\nabla} P \tag{1.1}$$

$$K = \begin{bmatrix} K_{xx} & K_{xy} & K_{xz} \\ K_{yx} & K_{yy} & K_{yz} \\ K_{zx} & K_{zy} & K_{zz} \end{bmatrix} \tag{1.2}$$

Where $\overline{u}$ is the volume- averaged velocity vector of the resin, η is the Newtonian viscosity of fluid, $\overline{\nabla} P$ is the pressure gradient vector, and K is the permeability tensor of the porous medium. This is a vector equation and can be expanded to its scalar form to relate the three components of the velocity to the permeability tensor which is second order symmetric tensor.

To characterize the permeability of a preform resin is injected into a dry preform and the flowrate and pressure drop across the resin domain is monitored. Two different injection modes can be used to measure the permeability; the linear (one-dimensional flow) and the radial (radial flow) injections methods. In the linear case, resin is injected from one side of the mold and fills an empty gap before entering the fiber preform. The results in one dimensional flow with a uniform flow front that moves along the length of the mold as the mold continues to fill. From this measurement, one can only find the permeability of the preform in the direction of the flow. The radial injection mode injects the resin into the mold from the center of the preform. The resin spreads radially. From this mode one can determine more than one component of the permeability sensor. Figure 1.2 depicts the two injection modes.

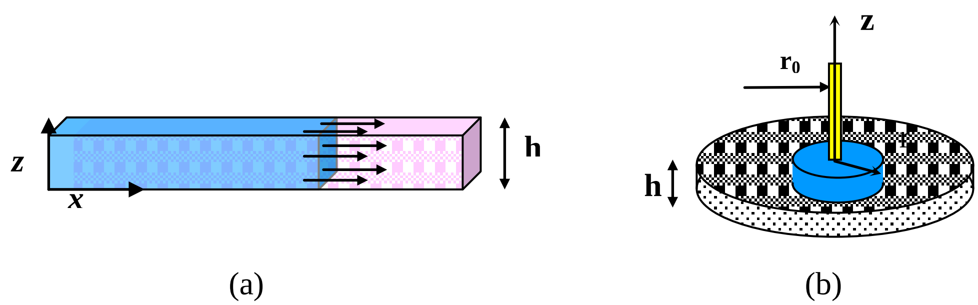

Figure 1. 2 : Schematics of (a) linear (b) and radial injections

Two-dimensional flow models work well to simulate the infusion of parts with small thickness. However, 3D permeability tensor is important where the flow process is three dimensional. This is usually the case when flow-enhancing ("distribution") media is used. This is common in Seemann Composites Resin Infusion Manufacturing Process (SCRIMP) as it speeds the resin flow on the surface of the part causing the flow to be three dimensional [5]. In this method as only vacuum pressure is used to drive resin to fill the mold and this could be very slow filling for large parts, a distribution media is placed on the top surface to enhance the flow in the in-plane direction but the flow is generally much slower in the through thickness direction which makes the flow field truly three dimensional requiring one to measure the permeability in the through thickness direction to simulate three dimensional flow. Third dimensional permeability is also important in RTM if the part to be molded is thick or if the injection is through one side of the preform (without making a hole that goes through the preform) and its through thickness permeability is at least an order of magnitude lower than the in plane direction.

Improving manufacturing technology is one of the greatest challenges for the liquid composite molding processes. Modeling and simulation in the last decade have shown that flow simulations are aiding in this process [6]. Hence there is a need to measure permeability of various preforms so the development and prototyping cycle time could be reduced as new preforms of glass, carbon and Kevlar or their hybrid combination is considered for different applications. One could use linear technique to characterize one component of the preform at a time or use the radial injection to characterize the in plane value [7]. Usually the through thickness permeability is characterized by performing a separate experiment [8]. An analytic technique was developed to characterize the permeability in 3 directions in a SCRIMP set up by Nedanov [3], however the error in the analysis due to the assumption that the injection was through an opening that was concentric and in the shape of the growing ellipsoid increased as the anisotropy of the ellipsoid increased.

The measurement of transverse permeability is more difficult because it is difficult to detect a flow front that moves perpendicularly to the laminate plane. The knowledge of the transverse impregnation behavior is still sparse and transverse permeability values have been determined for only a few fabrics.

Although the earlier work [3, 8-17] on measurement of transverse permeability is reliable, more ways are needed to determine transverse permeability. The contribution of this work is characterization of the full three dimensional permeability tensor from one experiment which is then useful for flow prediction for RTM flow when impregnating thick structural composite parts and in SCRIMP process in which the distribution media is used.

1.2 Objective and Thesis Outline

The objective of this thesis is to present a methodology to characterize the three dimensional permeability of a fibrous media from one experiment. The methodology couples the flow front data with a numerical simulation model and optimization technique to estimate the components of the 3D permeability tensor of the fabrics used in LCM.

In chapter two, previous work is discussed with respect to the methods for permeability characterization classified as analytical, experimental and numerical. In chapter three the proposed experimental method for the determination of 3D permeability tensor of fabrics from a single 3D radial flow experiments is presented. The proposed method involves experimental and numerical approach. The principle behind this technique is to compare 3D flow simulation resin arrival times to experimental resin arrival time at a number of locations. Permeability components are iteratively solved by matching the measured flow progression with the predicted ones by varying the permeability in the Liquid Injection Molding Simulation (LIMS) model iteratively until the error between measured and predicted values is a minimum. These sensors are not intrusive since they are embedded in the mold platen instead of the preform. This is a practical, fast and convenient method to determine 3D permeability of dry fibrous material.

In chapter four, validation of the new approach is presented via a numerical study using LIMS- in which any selected permeability values are used and flow front information at the sensor location is saved. Next only the information of at what time did the flow front arrive at each sensor is supplied to the newly developed methodology and the optimization routine which then provides the permeability values based only on this sensor information. These values are then compared with the permeability values that were used to generate the flow front information. Data sensitivity, limitation of the approach and results from real experiments are also presented in this section.

Finally, chapter 5 summarizes the conclusions and contributions of this thesis and puts forth suggestions for future work.

Chapter 2

PERMEABILITY CHARACTERIZATION METHODS

Darcy's law is a phenomenologically derived constitutive equation that describes the flow of a fluid through a porous medium. The law was formulated by Henry Darcy based on the results of experiments (published 1856) on the flow of water through beds of sand. It also forms the scientific basis of fluid permeability in fibrous media. In 1856, when Darcy [18] proposed his famous flow through porous media equation, he stated it in one dimensional form and introduced permeability as a scalar. The tensorial form of Darcy's equation [Equation (1.1)] was introduced by Liakopoulos [19, 20] in 1961. Three dimensional flows permeability is generally expressed as a symmetric second order tensor, written as follows:

$$K = \begin{bmatrix} k_{xx} & k_{xy} & k_{xz} \\ k_{yx} & k_{yy} & k_{yz} \\ k_{zx} & k_{zy} & k_{zz} \end{bmatrix} \tag{2.1}$$

One of its important properties is that there exists an orthogonal set of axes (principal axes) with respect to which all off diagonal terms of the tensor are zero. The principal permeability values can be represented by the quantities $k_{x'}$, $k_{y'}$ and $k_{z'}$. These quantities are used in determining permeability components with respect to arbitrary set of axes as in Equation 2.1 by coordinate transformation.

$$K = \begin{bmatrix} k_{x'} & 0 & 0 \\ 0 & k_{y'} & 0 \\ 0 & 0 & k_{z'} \end{bmatrix} \tag{2.2}$$

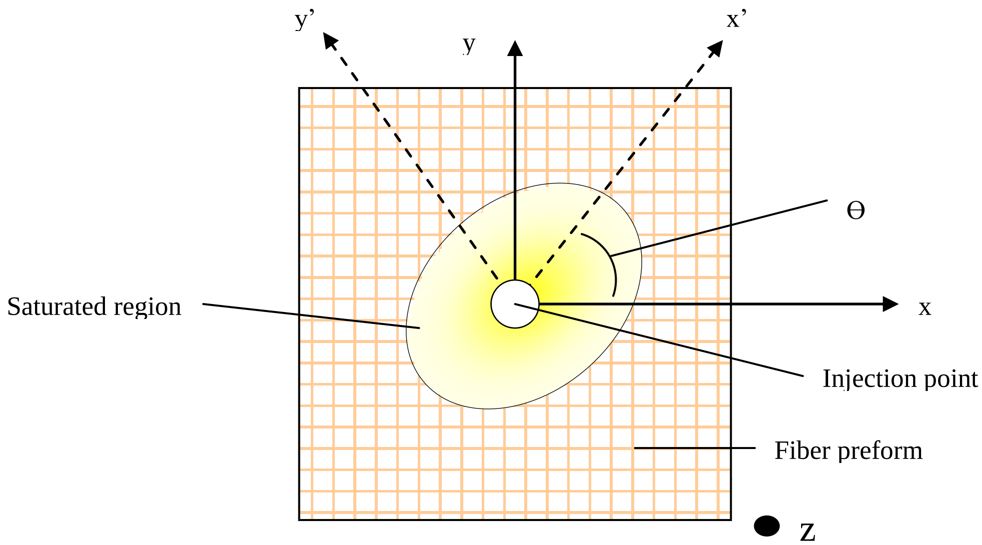

Figure 2. 1: Fluid flow front with x, y and z representing the mold coordinate system in which x′ and y' represent the preform in-plane principal axis

Continuous research efforts have been made since 1856 to establish reliable methods for permeability measurement and prediction [3, 8-17, 21-34]. In this chapter, a review of the existing methods for permeability characterization of fibrous porous media used in LCM is presented. The existing methods can classified as analytical, numerical and experimental.

2.1 Phenomenological Models Based on Analytic Method

Kozeny–Carman (KC) equation is the most famous permeability–porosity relation, which is widely used in the field of flow in porous media and is the starting point for many other permeability models. KC is the most well known analytical model developed for as an analytical expression for the permeability of granular media. It uses capillary model which assumes that the porous media consists of tortuous capillary channels with varying cross-section and the flow is governed by the Hagen-Poiseulle equation (laminar flow in pipes). However the introduction of the hydraulic radius concept into the capillary model [35, 36] resulted in the form of the Kozeny-Carman (KC) equation applicable to flow across fiber beds [37] and as shown in (Equation 2.3).

$$K = \frac{R_f^2}{4k_0} \frac{\phi^3}{(1-\phi^2)} \tag{2.3}$$

where K is permeability in one dimension (flow direction), R_f is the radius of the fibers, ϕ is porosity and k_0 is the Kozeny constant determined experimentally. Although the KC equation is widely accepted and used extensively, it has many limitations since its inception. Moreover, this equation is a semi-empirical relation and the KC constant is an empirical constant, which was proved to be not a constant and may be related to porosity [38]. The KC model has frequently been modified and has different modified versions to improve the estimation of permeability [39].

There are reported case of poor permeability estimates obtain using Kozeny –Carman equation for fibrous material. Ahn et al [12] reported a good agreement of permeability values obtain using Kozeny –Carman equation for woven fabric however Gauvin et al [29] showed that the equation describes inadequately the permeability of random mats. And in order to better describe the flow through fibrous media many researchers have proposed modifications to the “capillary model “. Also there are experimental studies [40, 41, 42] showing its unsatisfactory performance.

Gebart[30] proposed a geometric model for predicting permeability analytically. He derived expressions for permeability of an idealized unidirectional reinforcement consisting of regularly ordered, parallel fibers and was derived starting from first principles (Navier-Stokes equations) both for flow along and for flow perpendicular to the fibers. First, an approximate analytical solution for perpendicular flow is derived which differs from the Kozeny- Carman equation for the permeability of a porous medium in that the perpendicular flow stops when the maximum fiber volume fraction is reached. The solution for flow along the fibers has the same form as the Kozeny-Carman equation [30].

Bruschke introduced another predictive model for permeability of an idealized domain consisting of regular array of cylinders [43]. This model provides a closed form relationships matching asymptotically two limiting solutions: a lubricating solution for low porosities and a cell method solution for high porosities.

The limitation of Gebert and Bruschke models is that the physical model used to describe the system does not capture the structural details of real preform materials. The fiber preform usually used in LCM processes usually consist of woven or stitched fiber bundles known as tows or yarns, rather than of individual fibers and their geometric arrangements are usually more complex than the one assumed in analytic models.

Because of the complex structure of real fibrous materials most of these models mentioned and many others have limited applicability to idealized geometries (e.g. cylinder arrays) which do not resemble the structure of real preforms. Hence numerical and experimental methods are much more useful ways to characterize their permeability.

2.2 Numerical Models

Computational methods use well-defined cell geometry of the preform. The approach is to solve the NS equation with periodic boundary condition or use the Lattice- Boltzmann method to solve for the pressure drop by imposing a flowrate or imposing a pressure drop then solve for the average flow through the unit cell and then use Darcy’s law to back calculate the permeability of the unit cell. These are unit cells in the form of numerical or analytical models to predict flow through realistic structures. The way the geometric structure is modeled leads to different numerical methods. The applications of the Lattice–Boltzmann method and homogenization method as examples of numerical approaches to permeability prediction are presented here. And the analytical models use empirical relationships, capillary models and hydraulic radius theories to predict permeability of fibrous media.

2.2.1 Homogenization Method

In this method, the idea is to gloss over the variation of the heterogeneities and replace the heterogeneous medium by an equivalent homogeneous medium whose behavior over a macroscopic scale represents the averaged behavior of the medium. Several works have documented the mathematical base of the method [21, 22 and 34]. The numerical method solves the Navier-Stokes equations in a representative volume cell numerically. The homogenization method as in Figure 2.2 assumes that all physical quantities vary in local and global scales and the quantities are periodic with respect to the local scale due to the periodicity of the geometrical microstructure [44]

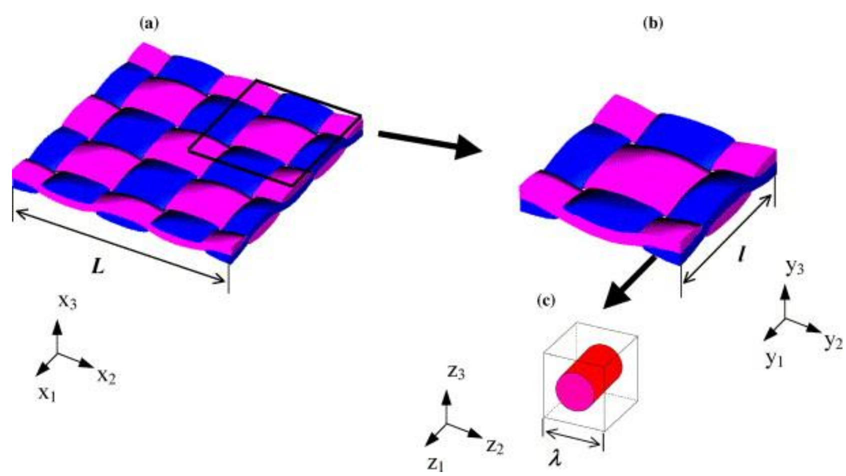

Figure 2. 2: Schematic diagram of homogenization method: (a) macrostructure of plain woven fabrics, (b) periodic macro-unit cell, (c) periodic micro-unit cell.[44] (with permission from Elsevier, publisher).

Chan and Kikuchi [23] presented a modeling and numerical simulation of a mold filling process in RTM using the homogenization method. They first derived the average flow model for the resin flow through a porous fiber preform and then extended the results to the case of double porous fiber preform. In another case, Dimitrovova and Faria [24] applied the homogenization method to RTM filling phase and performed the micro and macro level analyses. They calculated the average permeability of the cell numerically of the idealized bed consisting of aligned circular fiber tows and discussed the permeability determination for the single and double porosity case. The double porosity exists in preform where the spacing between the tows is about an order of magnitude higher than the spacing of the pores inside the tows. And in the case of single porosity the preform has a single flow level. All the cited research works used simplified idealized bed consisting of aligned fiber tows which is quite different from the real fabric because in modeling they start from a well-defined unit cell and assume such unit-cell repeats throughout the material. This does not account for the real dimensional fluctuations of fabric structure.

2.2.2 Lattice-Boltzmann Method

The Lattice Boltzmann Method (LBM) is based on microscopic models and mesoscopic kinetic equations. The fluid is imagined as a set of “fluid particles” moving and interacting on a lattice. The fictitious world, in which the particle velocity distribution function evolves, has the space, time and fluid particle velocities all-discrete. Although this representation is far from the richness of reality, it has been shown to be sufficient to recover the most important features of complex fluid flow [45].

The LB method has been used by several authors to study flow through various two-dimensional and three-dimensional porous media with varying degrees of complexities from computer-generated arrays of overlapping and non-overlapping , rhombs, spheres, rectangles, etc.[46- 50] to digital images of Fontainebleau sandstone obtained using a tomographic technique[51]. Martys and Chen [52] modeled the displacement of one fluid by another in a complex three-dimensional geometry, generated by using a tomographic image of sandstone. They utilized the method used by Shan and Chen [52] to model surface tension between fluids then calculated relative permeability in terms of saturation. Koponen et al. [25] employed the nineteen velocity LB model to calculate permeability of three dimensional random fibrous structure generated by a growth algorithm in discretized space. Dunkers et al [53] used optical coherence tomography to obtain images of the microstructure of a composite material. And in accounting for the dual porosity of the medium they used the model of Spaid & Phelan [54]. Koponen et al [29] studied the fluid flow in three dimensional fiber webs, where flexible fibers were placed randomly in the computational domain without overlapping. Nabovati and Sousa [27] investigated the permeability of sphere packs. Also Nabovati et al [28] reported their work on fluid flow in three-dimensional random fibrous media simulated using the lattice Boltzmann method.

The LB method overcomes the major limitation of the homogenization method. It is capable of simulating flow in realistic situations of complex fabric geometries and structure. However, Belov et al. [55] reported that the Lattice

Boltzmann calculations are computationally intensive. But it can also incorporate the surface tension effects of the fluid very easily.

Using numerical methods at the scale of the cell to represent the permeability of the entire preform has provided guidance but as the unit cells within a fabric may not all be identical the solution obtained with unit cells seldom match the permeability of the fabric that is measured. To perform an entire simulation within a preform with thousands of unit cells solving for Navier Stokes equation may be a computational challenge. Hence experimental methods are used to determine the permeability coupled with phenomenological methods since the permeability changes with fiber volume fraction; otherwise one would have to conduct many experiments for the same fabric to find the dependence on fiber volume fraction.

2.2.3 Experimental Methods

Several researchers have used an experimental approach to measure permeability. There are several classifications of these approaches. And an example of such classification can be based on the methods, which track the position of the flow front during impregnation with time and another record pressure drop or pressure history at different locations. The first method is known as unsaturated permeability measurement since it is mostly done by capturing the flow front position in the dry preform with respect to time. Saturated permeability is measured prewetting the fiber preform or measuring the pressure difference in the mold after a complete wet out

The method that tracks the position of the flowfront during impregnation by visualization can be further divided into intrusive and non-intrusive. The intrusive approach typically uses a particular type of sensor(s) placed in the mold while the non-intrusive record the flow front progression using a video camera. The shape of the flow is also used as means of classification: radial flow and unidirectional flow (1D or linear flow) experiments [56]. Also there is variation in experimental methods for measuring in-plane permeability and that for three-dimensional permeability. Many investigations have been conducted for determining the in-plane permeability of fiber preforms. However, permeability of a three-dimensional preform has not been investigated much and comparatively fewer contributions are available [57].

2.2.4 Methods for In-plane Permeability Measurement.

Two main experimental techniques have been used for measurement of in-plane permeability of fibrous media. These techniques involve two types of flow: unidirectional flow mode with liquid injected from a side gate; and radial flow mode with liquid injected from a central gate resulting in and proceeding following a circular or elliptical flow front. Figure 2.3 shows the schematic of the in-plane permeability measurement.

In the case of unidirectional flow the flow front position is measured and plotted as a function of time. From this data the permeability can then be calculated based on the integrated form of Darcy’s law arranged as shown in equation 2.4.

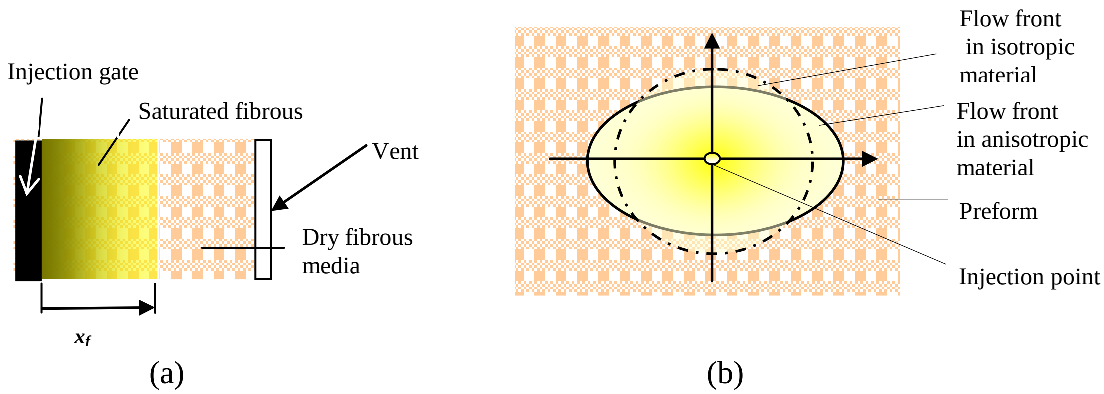

Figure 2. 3 : Schematic of in- plane permeability measurement (a) Unidirectional flow (b) Radial flow.

$$t = \left(\frac{1}{2} \times \frac{\mu \phi}{k \Delta p} \right) x_f^2 \qquad (2.4)$$

where t is the time since the start of mold filling, ϕ is porosity, μ is viscosity, Δp is pressure difference between inlet and flow front, and k is permeability with x_f is the flow front position. A plot of x_f^2 versus t is obtained with a straight line fitted to the data and the slope is used to estimate the permeability.

Many investigations have been carried out by researchers [29, 30, 32, and 33] on the unidirectional flow method. Parnas and Salem [33] proposed methods to obtain principal permeability and orientation using data from three unidirectional flow experiments. In using unidirectional flow experiments to determine the components of permeability tensor requires a number of experiments to be carried out which is a disadvantage of this method. And another disadvantage is racetracking, i.e. the preferential flow of the fluid along the mold walls when the material sample does not perfectly fit in the mold cavity.

The problems associated with unidirectional flow experiment do not exist in the case of radial flow experiment when determining the permeability of fibrous media. In the radial injection or 2D, the test fluid enters the material from a small circular gate within the sample and not from an edge as in the case of unidirectional flow. Similar to the unidirectional experiment the flow front position is recorded as a function of time. This part is slightly difficult to measure, because the flow front has an elliptical or circular shape depending on if the fibrous media is anisotropic or isotropic. In the case of isotropic material Adams et al [58] derived an expression by integrating Darcy's law as:

$$R_f^2(t) = \frac{2\Delta pt}{\phi\mu \ln(R_f / R_o)} k \tag{2.5}$$

where R_f is the flow front radius, R_o is the radius of the injection hole, k is the permeability, ϕ is the porosity, μ is the viscosity, and Δp is the pressure difference between injection port and flow front. Also for anisotropic materials Chan and Hwang [59] derived an expression for the equivalent permeability:

$$k_e = \frac{\phi\eta R_{01}^2}{4\Delta pt}\left(\left(\frac{R_1}{R_0}\right)^2\left(2\ln\left(\frac{R_1}{R_0}\right)-1\right)+1\right) \tag{2.6}$$

where $k_e = \sqrt{K_1 K_2}$ the equivalent permeability , R_1 the semi-major axis of the flow front ellipse which is half the distance across an ellipse along its long principal axis and R_0 is the radius of the circular injection gate, R_{01} is the equivalent gate radius in the direction of R_1 , Δp is the gauge pressure at the injection gate, and t is the time for the flow front to reach R_1 , ϕ is the porosity of the textile lay-up and η is the viscosity of the injected fluid. From the value of k_e and using the fact that the ratio of the major to minor axis is equal to the square root of the ratio of principal permeabilities , $\sqrt{K_1 / K_2}$. Permeability values determined by using unidirectional and radial flow experiment have been compared by several authors with mixed results. Some authors [60, 61] found a good match between the results obtained with different methods while other authors [32, 62] reported different permeability values using different methods. Repetition There have been many panel discussions on permeability measurements and the reliability of measurements at the International conferences for Flow Processes in Composite Material in 2004, 2006 2008 and 2010 at Newark, Delaware, Douai, France, Montreal, Canada and Ascona, Switzerland.

2.2.5 Transverse Permeability Measurement

As was had mentioned before when the flow is three dimensional one would like to characterize the permeability of the preform in the thickness direction as well. There are two methods for measuring the transverse permeability: (1) simultaneous measurement of all three principal values of the permeability tensor and (2) independent measurement of the in-plane and the transverse permeability values. The most common method to measure permeability in the out-of-plane direction is to use the one-dimensional channel flow apparatus (Transplane measurement device) with constant flow rate. To calculate the through thickness permeability, Darcy's law for one dimensional flow is used [11]. Several researchers have carried out experiments to determine the transverse permeability of fibrous media [38, 10, 14, 9, and 11]. Hee et al. [63] experimentally determined the out-of-plane transverse permeability based on channel flow through a circular tube with cross-sectional A and flow length, Q. They utilized the one-dimensional form of Darcy's law which relates the volume flow rate, Q, to the pressure gradient, dP/dz, in the direction of the flow:

$$Q = \frac{AK_z}{\eta}\frac{dp}{dz} \tag{2.7}$$

where $\boldsymbol{K_z}$ is the through thickness permeability , η viscosity.

Trevino et al. [9] used specially designed apparatus for transverse permeability measurement based on steady state unidirectional experiment. They measured pressure at the inlet and calculated permeability from one-dimensional form of Darcy's law. Wu et al. [10] measured the out- of- plane permeability from a one-dimensional flow model and a three-dimensional flow simulation.

Ahn et al. [12] designed a device to measure simultaneously measure the transverse permeability and capillary pressure under transient conditions. They measured the position of the flow front as a function of time and used the integrated form of Darcy's law shown in Equation 2.4.

2.2.6 Three-dimensional Permeability Measurement

In order to fully characterize a fibrous media there is need to determine its three-dimensional permeability in the case of materials with isotropic and anisotropic in-plane permeabilities. And there are only few scientific contributions describing 3D-flow experiments to fully characterize the permeability tensor in a single experiment. Resin transfer molding, RTM, is a well established molding process for small and thin components , there are still a number of practical problems when utilizing RTM to thick components. One issue is the reliable and economical measurement of three-dimensional permeability [11].

Woerdeman et al. [14] presents a general methodology to determine the components of the three-dimensional permeability tensor from a set of one-dimensional saturated flow experiments. The results are obtained by solving numerically six highly nonlinear algebraic equations relating the effective permeability to the permeability tensor [3].

Weitzenbock et al. [11] detected flow front using thermistors and described the difficulty caused by the capillary pressure in three-dimensional permeability measurement. In another work Ballata et al. came up with another flow monitoring technique, which makes use of new sensor technology called Smart Weave [57].

Ahn et.al. [12] are using the same measurement principle as Weitzenböck. The experiments were performed with corn oil as test fluid. The 3D-flow is monitored by embedded 3D- fiber optic sensor grids inside the preform. Tests were performed to demonstrate the usefulness of fiber optic sensors in monitoring fluid flow and in determining the permeability. The relatively small size of the optic sensors has a negligible influence on the fluid flow, but this relatively new LCM-monitoring technique is still invasive.

Gokce et. al. [64] presented a new experimental permeability estimation method, called the Permeability Estimation Algorithm (PEA) that uses a numerical process model instead of analytical relationships. They obtained the flow front information using camcorders, and the accuracy of PEA was validated in a virtual experiment. The approach is limited to finding the preform permeability in the thickness direction and of the in-plane distribution media (DM), a high-permeability fabric. Its application is in vaccum assisted resin transfer molding (VARTM).

Bréard et al. [65] describe the 3D-flow of a resin through a reinforcing material. The flow monitoring system is based on X-ray radiography technique. This monitoring technique is not commercially applicable because of its high cost, but can show interesting phenomena as for example deformation of the fiber reinforcement material in the injection area, which occurs during 3D-injection. It is not reported if this technique is reliable for 3D-permeability measurements.

Nedanov et al. [3] propose a method for simultaneous determination of the principal values of the three-dimensional permeability tensor of fiber preforms.
The experimental set-up consists of an electronic balance and a video camera capable of recording the mass flow and the in-plane flow front evolution. Nedanov's measurement method is based on visual monitoring of the in-plane flow front position. The shape and size of the in-plane flow front through the transparent membrane as

well as the amount of fluid in the preform and elapsed time are recorded and allow characterizing the three-dimensional flow front evolution. The mathematical model proposed, based on Darcy's law, and describes the case of a three-dimensional flow with a point as injection gate.

Each of these experiment approaches has their disadvantages. The use of embedded sensors affects the pattern of flow and renders the experimental data unreliable. Weizenbock [11] observed that the flow front in the part of the mold where the thermistors sensors had been placed was lagging behind compared with other undisturbed parts of the mold. Also since the sensors are normally embedded in the preform manually, this requires time and effort. Numerous experiments are usually required for reliable characterization of preform permeability and as such using embedded sensors will require extensive time and labor rendering the methods less efficient. And the method [65] that involves the use of X-ray spectroscopy to measure the flow front through the thickness is rather expensive. In case of Nedanov experiments, the results for through thickness could be unreliable as they used only one data point to find the transverse permeability –which was when the arrival of the resin was recorded at the bottom. Also the size of the gate had an effect on the permeability calculations.

From the review of the existing experimental methods for permeability characterization of fibrous media shows that while traditional methods for in-plane permeability measurement are well developed the methods for transverse permeability measurement need further investigation. Hence the need for reliable and fast method to determine the components of the three-dimensional permeability tensor in a single experiment and using simple equipment is desirable. The objective of this research is to develop and validate such an experimental method.

Chapter 3

NEW METHOD TO MEASURE THREE DIMENSIONAL PERMEABILITY

This chapter will present a new method for the determination of 3D permeability tensor of fibrous media from a single radial flow experimental which can report the resin arrival data via electrical resistance sensors embedded in the top and the bottom plate of the mold. The proposed method uses an optimization routine in which the permeabilities in a 3D flow simulation of the identical mold is updated continuously until the error between the simulation arrival times at all the 192 sensor locations and the experimental arrival time is minimum. The optimization routine systematically changes the values of the components of the permeability tensor using golden search method until the best match of the flow pattern is obtained.

3.1 The Experimental Set-up

The experimental set up being described and used in this work is based on the work of Qiang Liu and Richard S. Parnas [66] except for the fiber shear resistance guard. The mold along with the sensors was built by Dr. Parnas and provided to use for further investigation.

3.1.1 Hardware

Both top and bottom mold plates are made of stainless steel, 40 cm long, 40 cm wide, and 3.2 cm thick (Figure 3.2). On the back of the plates, 16 channels 1.9 cm wide were milled at angles every 22.5^o. On it are located 16 radial lines of sensors at 0, 22.5, 45, 67.5, 90, 112.5, 135, 157.5, 180, 202.5, 225, 247.5, 270, 292.5, 315, and 337.5^o . Each radial line of sensors has six evenly spaced sensors inserted into the channels through the mold wall to detect fluid arrival times. The spacing between the sensors along each radial line is 1.91cm with the innermost sensor located at 4.13 cm from the injection hole. Thus there are 96 sensors in the top and both plate each for a total of 192 sensor data that can be collected during the injection process. The sensor pattern is illustrated in Figure3.2. The back end of the sensor is soldered to a ribbon cable, which is connected to the data acquisition (DAQ) cards inside the computer. Two cards (Measurement Computing Corporation PCI-DIO 96 (3 counters 16-bit) are used, one for the top plate and one for the bottom plate.

There are 96 digital channels on each card, permitting 96 sensors in each plate. In the center of the top plate, a sensor is positioned to detect when the incoming fluid reaches the top plates providing the time for the fluid to go through the thickness. The bottom plate looks similar to the top plate shown in Figure 3.2, but there is a fluid injection port in the center of the bottom plate. The radius of the injection port is about 2.5 mm. The fluid is pumped into the equipment by the laboratory central pump system under constant positive pressure of 1bar. The experiment is monitored and controlled through LabView software. The sensor trigger times from the top plate and from the bottom plate can be collected and analyzed together. The fluid used in our experiment is diluted corn syrup (DCS), made of distilled water and corn syrup from Archer Daniels Midland Company (ADM) (42 DE Corn Syrup (1430)). The average viscosity used is 0.1 Pas (100cp) at room temperature. This DCS fluid is Newtonian in the shear rate ranges used for typical experiments [56].

The sensors embedded in the top and bottom plate (Fig 3.2) are pieces of copper wire with PVC (polyvinyl chloride) and nylon insulation, fixed into the mold plate through a small screw. An O-ring is compressed when the sensor is screwed into the plate, sealing the mold and locking the sensor wire into place. The hole diameter in the sensor plate for each sensor is 3.03 mm, to accommodate the solid copper wire (2.06 mm or 0.081in diameter), the PVC insulation (0.38 mm or 0.015in thick) and a nylon jacket (0.10 mm or 0.00400 thick).

These holes do not disturb the flow because the sensor is inserted and ground to form a smooth flush surface with the plane of the surface of the mold platen (Figure *3.1)*. During an injection, the electrically conductive fluid covers the insulation between the sensors core wire and the mold plate, creating an electrical connection and generating a trigger signal for the data-acquisition system. An electrical circuit was configured to generate a large change in potential when fluid covers the sensor, permitting digital communication with the computer. The complete experimental set-up is shown in Figure 3.2

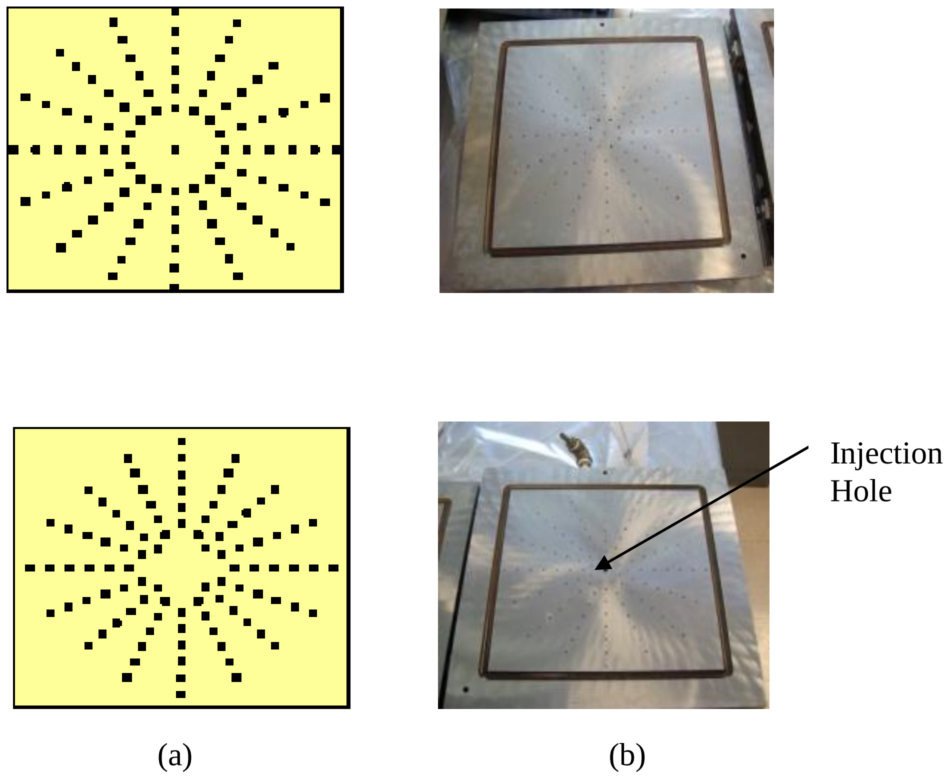

Figure 3. 1 : The top and bottom plate of the mold plates showing the locations of the sensors and the injection gate (a) Schematic (b) Mold plate.

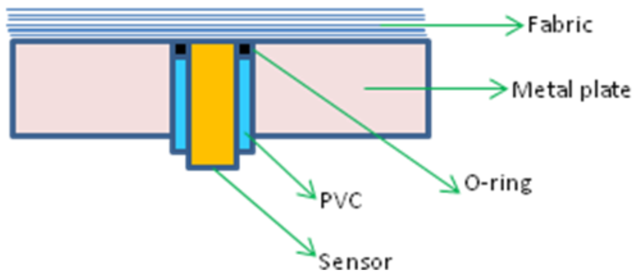

(a)

(b)

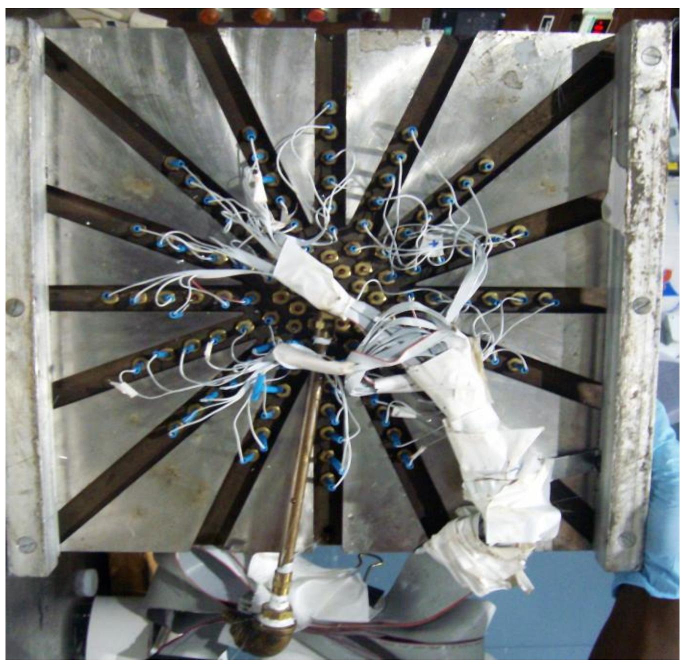

(c)

Figure 3. 2: Radial Injection Mold (a) Schematic of the position of the sensor (b) sensor (c) bottom view of the bottom sensor plate

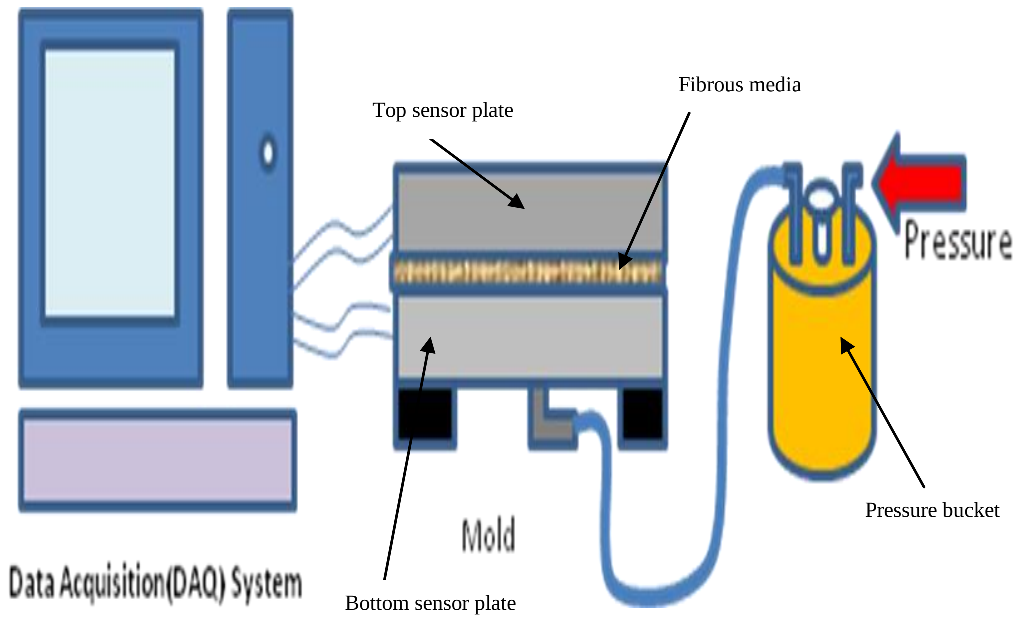

Figure 3. 3: Schematic of the Experimental set-up

3.1.2 The Software

The software was written using LabVIEW and MCC's Universal Library for LabVIEW. The latter contains a set of programs that allows LabVIEW to communicate with the data acquisition board. The software deals with data coming from 96 sensors on each board. The 96 sensors are mapped by two numbers, their port number and bit number. The software records the arrival times at the sensors and stores it in a CSV file (Coma separated value) with the coordinates of the sensors. The procedure can be interrupted by the operator by clicking on a button on the LabVIEW VI's front panel. Ideally, the data acquisition should be started and stopped by the fluid triggering the sensors on the inner and outer circle. It is crucial not to let the acquisition continue after the first outermost sensor is triggered. Once the outermost sensor is triggered the fluid will have reached the boundary of the mold which will act like a vent offering no resistance to fluid flow. This will affect the results of the arrival times at the sensors after that time. The mapping of the sensors by the LabView program can be seen as in Figure 3.4.

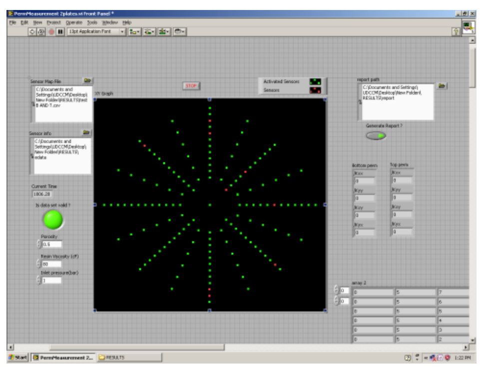

Figure 3. 4: Labview mapping of the 192 sensors in a planar view on the user interface. There are 16 radial lines each containing 6 sensors on the plate. All the 12 sensors, six from the bottom and the top plate are shown here on all of the 16 radial lines.

3.1.3 Fiber Shear Resistance Guard

Accurate placement or alignment of the fiber layers is very important to obtain accurate results. Some systematic asymmetry of the arrival times in preliminary experiments was found to be due to the misalignment between fiber layers and the circular hole in the center of the bottom. This problem was resolved by using fiber shear resistance guard made from open cell Quick-Recovery Super-Resilient Polyurethane Foam. Also known as Poron®, this high-performance foam has the quickest recovery from compression - even after extended use. This material is shown in Figure 3.5.

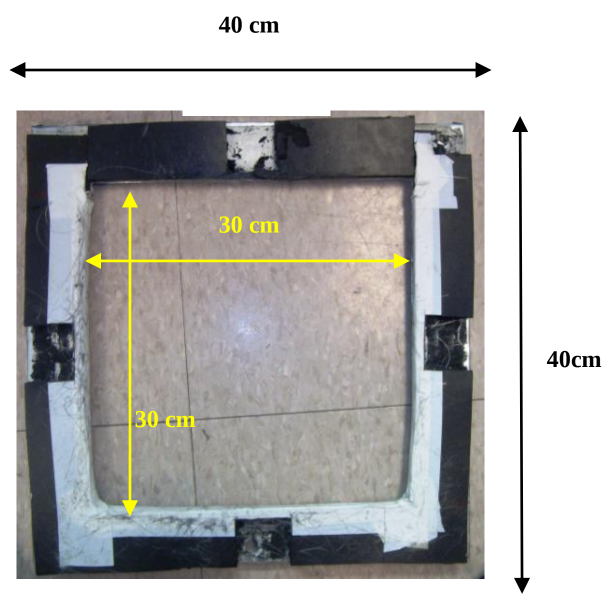

Figure 3. 5: Fiber shear resistance guard

3.2 Liquid Injection Molding Simulation (LIMS) Model

Liquid Injection Molding Simulation (LIMS) is a software tool that simulates the mold filling stage of resin transfer molding (RTM) and related processes by modeling flow through porous media by Finite Element / Control Volume Method.

The LIMS model is a 3D mesh with an injection line. The mesh was built in a way so that there are nodes on the radial line that correspond to the locations of the sensors on the plate. LIMS can be described as a dedicated finite element/ control volume based simulation of flow through porous media, capable of analyzing both 2-D and 3-D flows [67, 68]. LIMS uses the permeability tensor as the input and provides the arrival times of the resin at each node once the appropriate boundary conditions are set at the injection port.

The mesh has an outer radius of 0.15 m and circular inlet radius of 0.0025 m. In choosing the right mesh various mesh sizes were considered. In Figure 3.6(a) time to fill a specific outer node with coordinate (x, y, z) = (0.15, 0, 0) m was plotted with respect to the total number of nodes in the mesh. A choice of mesh size with 3000 nodes was made which has node fill time which is 0.2% less than that of the converged solution.

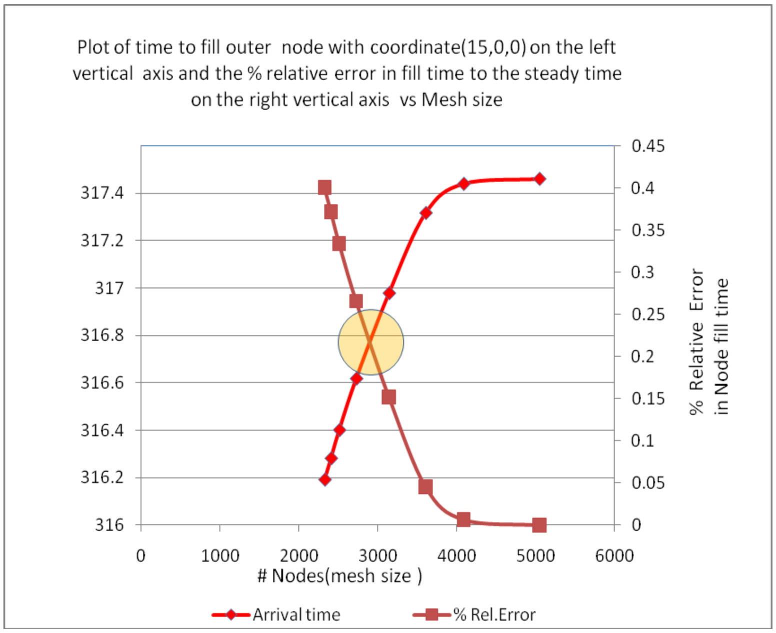

(a)

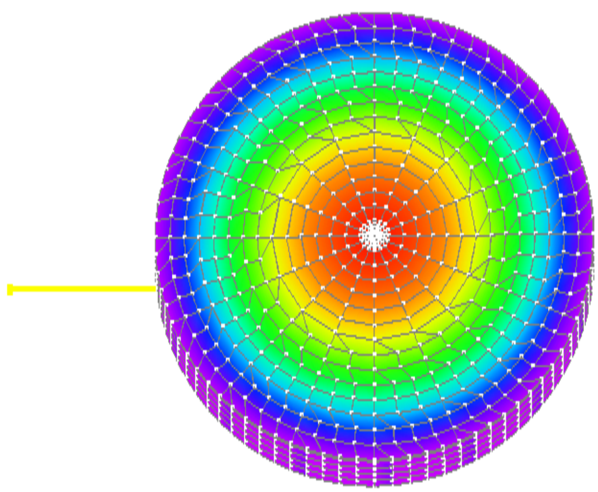

(b)

Figure 3. 6: (a) The plot showing convergence of node fill time vs the 3D mesh size. A mesh with 3000 nodes was selected as it is within 0.2% of the converged solution (b) Selected LIMS 3D mesh with 3000 nodes for flow simulation with numerical sensors at the same locations as in experiments.

3.3 Golden Section Search Minimization Technique

3.3.1 Residual Sum of Square

Residual sum of squares was used to qualify the difference between the experimental and simulated arrival time at a certain sensor location. The technique minimizes the sum of squares of the residuals, RSS, between the experimental flow arrival times and the simulated flow arrival times at each corresponding sensor and the node corresponding to that sensor location. RSS is a measure of the discrepancy between the experimental data and the simulated data as shown below

$$RSS = S_r = \sum_{i=1}^{N} \left((T_{i,\exp} - T_{i,\lim s})^2 \right) \tag{3.1}$$

where RSS is residual sum of squares, N is the total number of sensors, *i* is the sensor number, $T_{i,\text{ exp}}$ experimental time to fill the *i*th sensor and $T_{i,\text{ limps}}$ simulated time to fill the *i*th sensor. A small RSS indicates minimal error of the simulated results to the experimental data. This minimum is calculated for all permissible combinations of permeability components in the simulation. As the multivariable optimization may be time consuming, a sensible and efficient technique has to be selected.

3.3.2 Multivariable Fit Technique

The Golden Section Search has been chosen to be used in this implementation. The technique minimizes the sum of squares of the residuals, RSS, between the experimental flow arrival times and the simulated flow arrival times at each corresponding sensors in the experiment and the node representing the location of the sensor in the simulation by repeating a sequence of univariate minimizations for each permeability component. Univariate in this context means that the permeability component being optimized is a variable while other permeability components are held constant.

Generally, the Golden Section Search Minimization Technique (G2SMT) is a technique for finding the extremum (minimum or maximum) of a unimodal function by successively narrowing the range of values inside which the extremum is known to exist. As two boundary and two inner points within the interval are needed to determine the next interval, their location is chosen so that only one new location is chosen in each step, one internal point becoming a new boundary and one internal point is retained. This minimizes the number of functional evaluations, which is quite important as a single evaluation requires one to simulate the entire radial flow experiment. To illustrate how the golden ratio is determined let us consider the three points in Figure 3.7 based on two conditions [69]

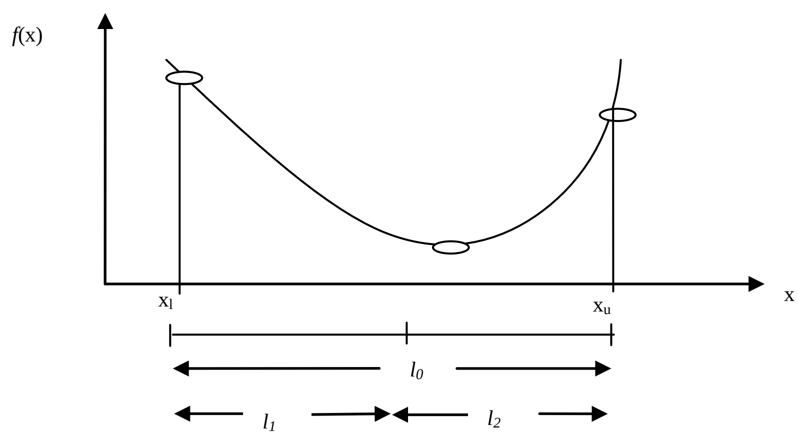

Figure 3. 7: Determination of the Golden ratio, R

The first condition specifies that the sum of the two lengths l_1 and l_2 must equal the original interval length as expressed below:

$$l_0 = l_1 + l_2 \tag{3.4}$$

The second condition requires that the ratio of the lengths must be equal as expressed by the following equation.

$$\frac{l_1}{l_0} = \frac{l_2}{l_1} \tag{3.5}$$

Equation 3.4 can be substituted into Equation 3.5 and denoting l_2/l_1 by R we arrive at the following expressions:

$$R^2 + R - 1 = 0 \tag{3.6}$$

This can be solved for the positive root known as the golden ratio as follows.

$$R = \frac{\sqrt{5} - 1}{2} = 0.61803........ \tag{3.7}$$

This technique is used to optimize the permeability values of the fibrous media for each component of the permeability tensor in a sequential way. The R value ensures proportionate subdivision of the bound where the minimal value is known to exist.

Figure 3.8 illustrates a single step in the technique to find the minimum. The sum of the squares of the residual, RSS, between the experimental arrival times at the sensors and the corresponding LIMS arrival time at the node are on the vertical axis, and the horizontal axis is the estimate of the permeability value, P. The value of S_r has already been evaluated at three points: P_1, P_2, and P_3. Since S_{r2} is smaller than both S_{r1} and S_{r3}, it is clear that a minimum lies within the interval from P_1 and P_3. Subsequently only one value of S_r is evaluated in each iteration while three values come from the previous iteration.

The next step in the minimization process is to "probe" the S_r by evaluating it at a new value of P, namely P_4. It is most efficient to choose P_4 somewhere inside the largest interval, i.e. between P_2 and P_3. From the diagram, refers to the figure, it is clear that if the function yields S_{r4a} which is higher than S_{r2} , a minimum lies between P_1 and P_4 and the new triplet of points will be P_1, P_2, and P_4. If the function yields the value S_{r4b} which is lower than S_{r2} then a minimum lies between P_2 and P_3, and the new triplet of points will be P_2, P_4, and P_3. Thus, in either case, we can construct a new narrower search interval that is guaranteed to contain the permeability value for which the time residual sum of squares S_r is minimum.

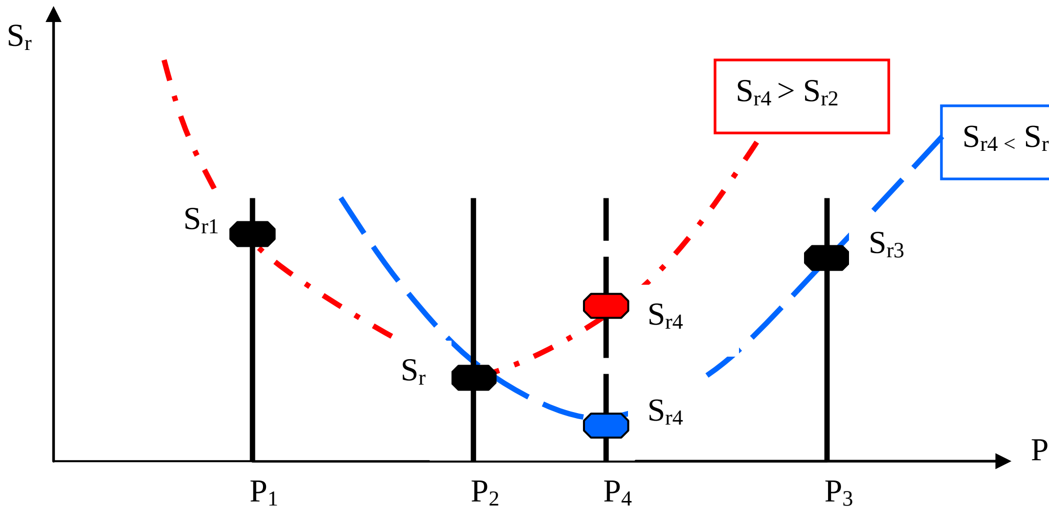

Figure 3. 8: Golden section minimization scheme

3.3.3 Selection of the Starting Values

Before beginning the optimization procedure it is necessary to generate starting values. In practice the convergence region of most optimization methods is limited; if the starting values are selected outside a certain region the method may not converge to the desired optimum. Even if there is convergence, the final result still may depend on the permeability starting values if the function has local minima. In the cases we examined, there is only a single minimum within wide region , 1e-17 to 1e-6 m^2, but the convergence speed still depend on the initial value. The permeability (Kxx, Kyy, Kxy and Kzz) prediction sequence is Kxx first then Kyy, followed by Kxy and Kzz is varied last. For each step there is a need to specify the range to look for the value and this can be done after calculating the initial permeability values. Then the range is selected as at least- two orders of magnitude above and below these guess permeability values. The program uses P_1 and P_3 to calculate P_4 and P_2 based on the golden ratio. Before the first search is initiated the estimate for three *RSS* values at P_1, P_2 and P_3 are needed. Four initial permeability values, *Kxx, Kyy, Kxy, and Kzz,* initial values are required for the G2SMT to execute. And these are calculated by using the equations derived by Weitzenbock et. al [11] for principal permeabilities.

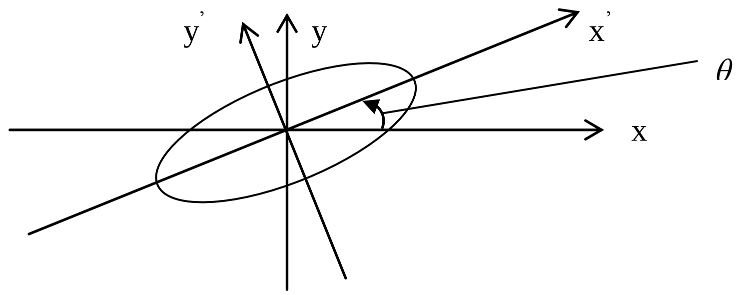

Figure 3. 9 : In-plane flow front diagram showing the angle between the preform principal axes and the mold axes. The angle is used to guess $K_{xy'}$ as shown in Equation 3.11

$$K_{x'} = \frac{\mu\varphi}{6\Delta P}\left[\frac{2x'^3_f}{r_{o,\mathrm{mod}}} - 3x'^2_f + r^2_{o,\mathrm{mod}}\right]\frac{1}{t_{fx'}} \tag{3.8}$$

$$K_{y'} = \frac{\mu\varphi}{6\Delta P}\left[\frac{2y'^3_f}{r_{o,\mathrm{mod}}} - 3y'^2_f + r^2_{o,\mathrm{mod}}\right]\frac{1}{t_{fy'}} \tag{3.9}$$

$$K_{z} = \frac{\mu\varepsilon}{6\Delta P}\left[\frac{2z^3_f}{0.1r_{o,\mathrm{mod}}} - 3z^2_f + (0.1r_{o,\mathrm{mod}})^2\right]\frac{1}{t_{fz}} \tag{3.10}$$

$$K_{xy'} = \frac{1}{2}(K_{y'} - K_{x'})Tan\theta \tag{3.11}$$

Two positive definite conditions $\left(K_{x'} > 0 \ \ and \quad K_{xy'} < \sqrt{K_{x'}K_{y'}}\right)$ must be satisfied for guess permeabilities to be used, where $K_{y'}$ *=GPY (*Guessed Principal permeability values in the y-direction), $K_{x'}$ *=GPX(* guessed principal permeability values in the x-direction) , K_z *= GPZ (*guessed principal permeability values in the z-direction *)* and $K_{xy'}$ *=GPXY.* And *h*, thickness of stacked fiber layers at the specified fiber volume fraction , *P*, injection pressure, $r_{o,mold}$, radius of the injection hole, $t_{fz'}$ experimental flow front arrival time at the sensor with coordinate((0, 0, z'_f), $t_{fx'}$ experimental flow front arrival time at one of the outer sensors on the principal axis-x', $t_{fy'}$ experimental flow front arrival time at one of the outer sensors on the principal axis-y', x'_f experimental flow front position of one of the sensors on the principal axis-x', y'_f experimental flow front position on the principal axis- y', μ viscosity , and φ is the fiber volume fraction. The limits, P_1 and P_2, for K_{xx}, K_{yy}, K_{zz} are chosen based on the values *GPX*, *GPY*, and *GPZ* respectively. Select P_1 to be least two orders of magnitude below *GPX, GPY, GPZ and GPXY* while P_3 at least two order of magnitude above. The program will use the values of P_1 and P_3 to calculate P_2 and P_4 in each case.

3.3.4 The Convergence Criterion

The iteration loop of the optimization method is terminated when the convergence criterion is met. The convergence criterion programmed in G2SMT is based on the evaluation of the least square formulation of the difference between the experimental and the numerical flow front arrival times. And specifically the iteration loop is said to converge when the relative error between prior sum of square of the residual , RSS_k and the current one, $RSS_{k+1,}$ is within 2% and unchanged with further iterations and where *k* is the *k*th iteration.

3.3.5 Overview of Permeability Prediction Using Flow Simulation

The goal is to determine the permeability components from experimental values by matching the measured flow progression with the predicted ones at the sensor locations as the permeability values in the LIMS model are varied according to the golden section optimization technique. The algorithm flow chart and procedure are shown in Figure 3.10 and 3.11 respectively and is briefly described below

- Initial step

Based on the initial permeability guess and the upper and lower bound LIMS simulate the 3D flow for all relevant scenarios and records the arrival time at the corresponding nodes to that of the experimental sensors. The sum of squared residuals between the LIMS arrival time and that of the experiment is then calculated at each point and iterative minimization is started.

- Iterative steps

G2SMT will now use the previous permeability result set and follow the procedure described in Figure 3.9 to obtain new, closer set of permeability values. This is achieved on univariate basis: First, Kxx is improved to find optimal value for existing guesses for Kyy, Kxy and Kzz. Each iteration step optimizes all the values in sequence. These are input as materials data in LIMS which will run the simulation again and record the new arrival times. The sum of squared residuals between the

LIMS arrival time and that of the experiment is now calculated and compared with that of the previous values. The interval is then reduced as described above. The procedure is continued until the residual sum of squares does not change for two consecutive iterations. Then, RSS is optimized by changing Kyy maintaining the other values to be the same. This procedure is repeated to find Kxy and then Kzz. Thus within single iteration, four iterative searches are carried out, one to optimize each unknown component of permeability. And specifically that iteration loop is said to converge when the relative error between prior sum of square of the residual , RSS_k and the current one, $RSS_{k+1,}$ is within 2% and unchanging with further iteration and where k is the kth iteration as shown in Figure 3.12 below.

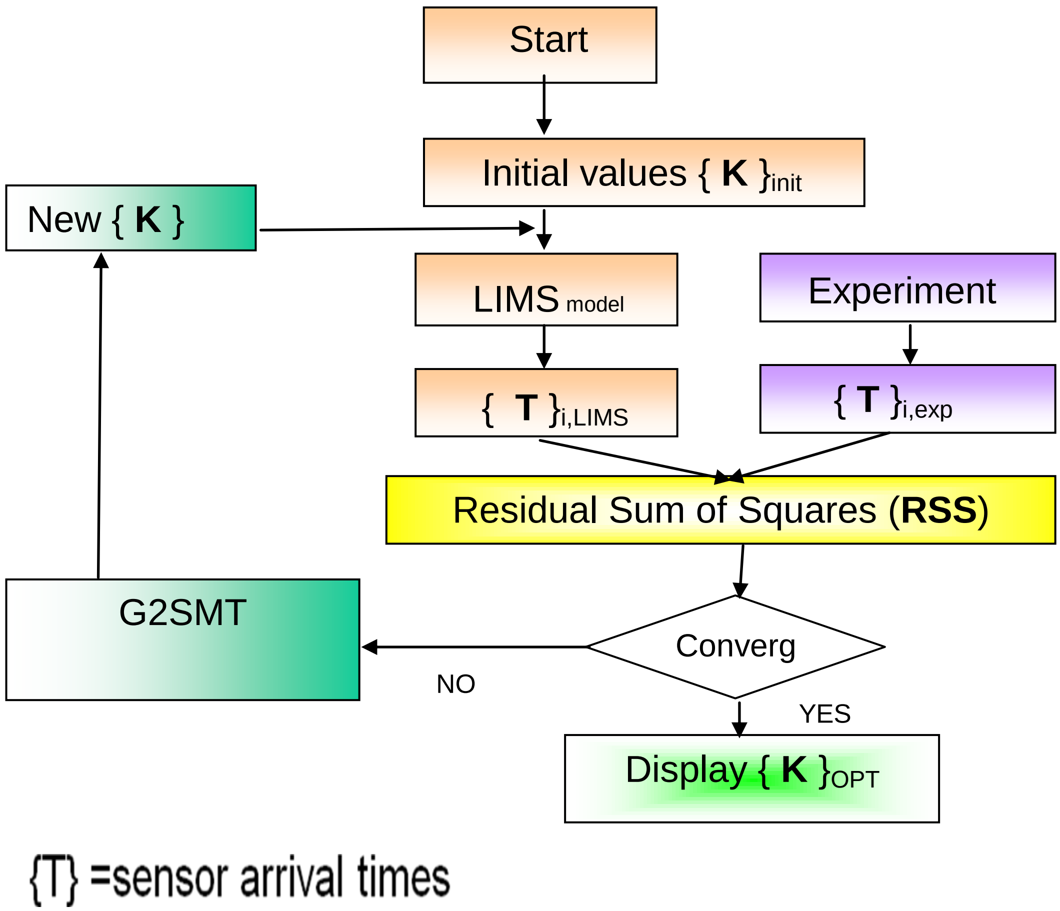

Figure 3. 10: Flow chart to determine permeability values by comparing the experimental data with numerical simulation in which the permeability is varied using golden section search method until the error between the experimental data and numerical predictions is minimized.

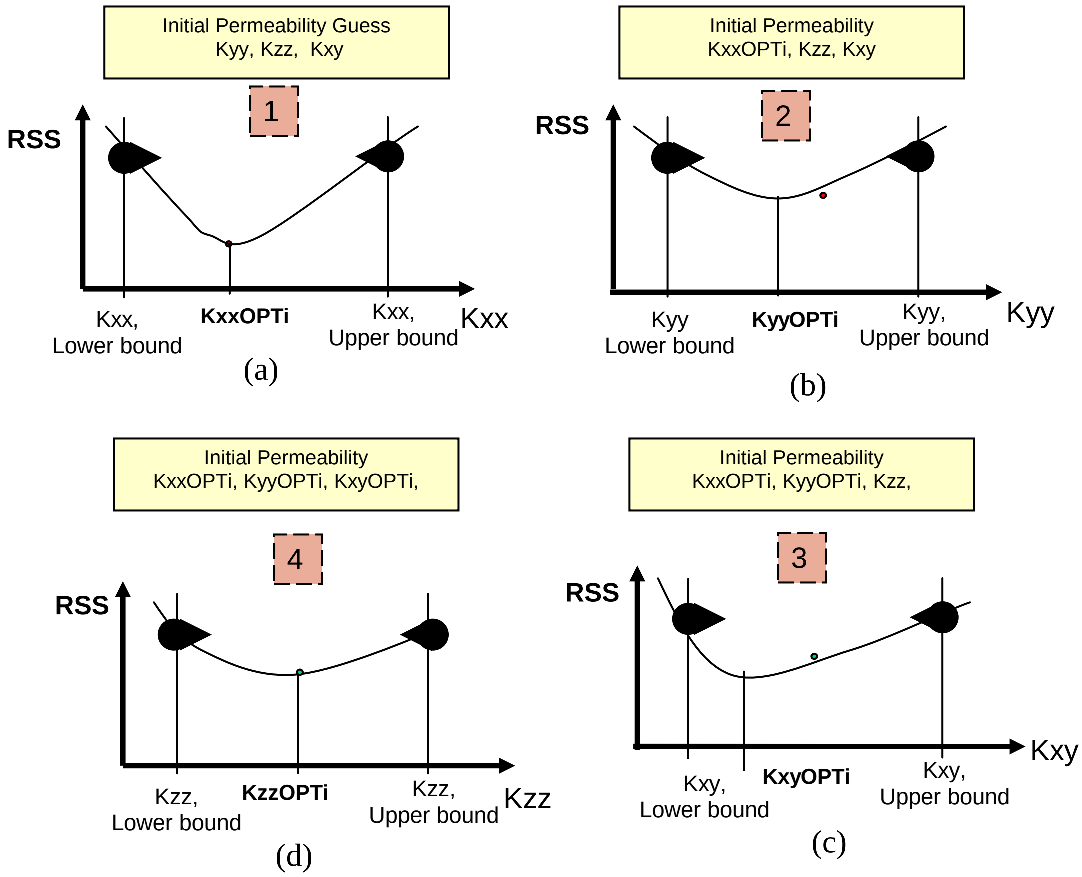

Figure 3. 11: Uni-variate determination of permeability using flow simulation

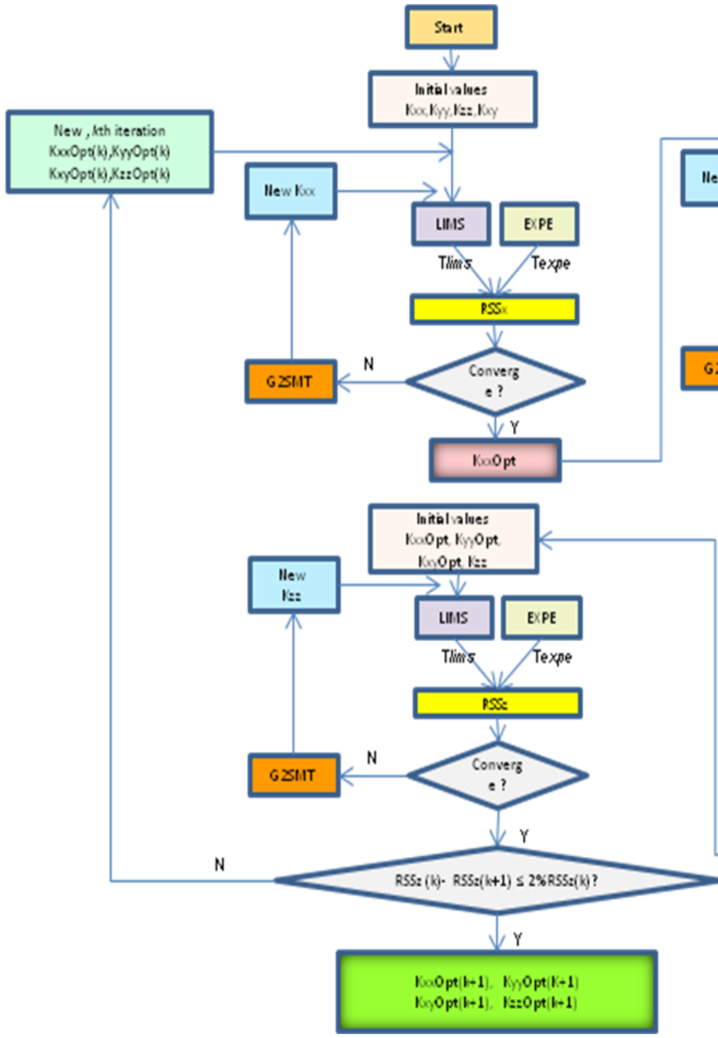

Figure 3. 12: Flowchart showing the optimization routine to predict Kxx, Kyy, Kxy, Kzz permeability values in sequence.

Chapter 4

VALIDATION OF PERMEABILITY CHARACTERIZATION TECHNIQUE

The technique proposed relies on the accuracy of the numerical method, the inverse approach used to find permeabilities with over prescribed conditions and various sensitivities in collection of the data. This chapter explores the validity and accuracy of the method proposed.

4.1 Numerical

4.1.1 3D Permeability Prediction Accuracy

The accuracy and fidelity of the method described in the previous sections was evaluated numerically. In actual experiments, the permeability of the same preform will vary a few percent even after utmost care as one cannot control the nesting between different layers of the fabric and there may be slight variations in the fabric architecture, hence they may not be the best candidate to validate a new technique. Hence we use a virtual filling of the mold to verify our method. A simulation of the experiment is run by selecting the permeability values and recording the arrival times at the nodes corresponding to the coordinates of the sensors in the experimental set-up are obtained. Now pretending that this is our "experimental resin time data"(virtual experiments) we use the algorithm developed in Chapter 3 to find the permeability values and then compare them with the ones we used to simulate the experimental run. The evaluation was carried out for two cases (1) Transversely isotropic (2) Transversely anisotropic preforms. Wide and narrow range in which the extrimum is known to exist was considered. Also starting permeability values i.e., the initial guess close and far away from the permeability used in the numerical experiments was studied. The results of the experimental study shows that permeability values of fibrous media can be determined by matching simulated flow front to that of the experimental. The summary of the study is presented in Table 4.1 and Figure 4.2 and Figure 4.3.

Table 4.1 shows the permeability values used for the numerical experiment and the predicted permeability values for the same experiment. And in Figure 4.2 and 4.3 the plot of optimized permeability value versus the number of iteration required to reach convergence is shown. The study is for the cases of anisotropic (both for the cases where principal axes coincident with the mold axes or not) and isotropic materials.

Table 4. 1: Parameters for numerical experiments

Parameter	Value
Mesh outer radius, m	0.15
Mesh inner radius, m	0.0025
Porosity	0.5
Viscosity , Pa·s	0.1
Injection Pressure, Pa	100000
Mesh 3D elements	2304

Mesh 1D elements(represent the tube)	17
Mesh elements	2321
Mesh nodes	2887
Mesh thickness, m	0.006
Radius of injection tube,m	0.009
Length of injection tube, m	4.318

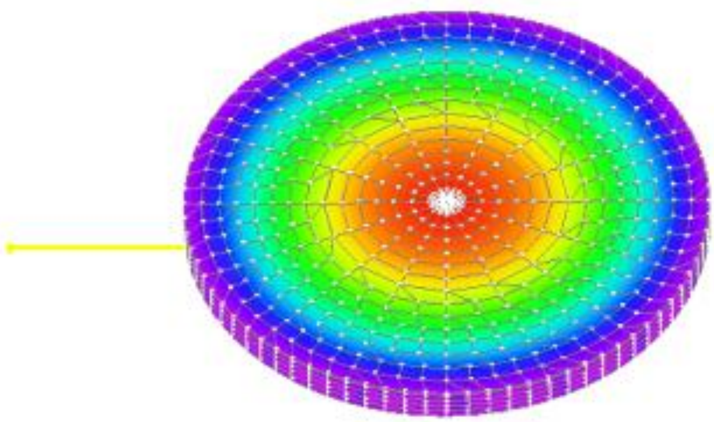

Figure 4. 1: LIMS Model: 3D mesh for flow simulation with numerical sensors at same locations as in the experiment.

Table 4. 2: Isotropic Case: Comparison of permeability values supplied to LIMS with those predicted from the numerical experimental data

Numerical experiment	Initial search range (L- U) m^2	Permeability	Values supplied to LIMS, m^2	Predicted value m^2	Relative error (%)
1	1e-12 - 1e-9	Kxx	6.00E-10	5.99E-10	0.205
	1e-12 - 1e-9	Kyy	6.00E-10	5.99E-10	0.222
	1e-13 - 1e-10	Kzz	3.00E-12	3.00E-12	0.047
2	1e-12 - 1e-9	Kxx	6.40E-10	6.40E-10	0.052
	1e-12 - 1e-9	Kyy	6.40E-10	6.40E-10	0.056
	1e-13 - 1e-10	Kzz	3.60E-12	3.61E-12	0.153
3	1e-13 - 1e-8	Kxx	1.00E-11	1.01E-11	0.807
	1e-13 - 1e-8	Kyy	1.00E-11	1.01E-11	0.799
	1e-15- 1e-9	Kzz	3.40E-13	3.44E-13	1.265
4	1e-15- 1e-9	Kxx	1.60E-08	1.61E-08	0.625
	1e-13 - 1e-7	Kyy	1.60E-08	1.61E-08	0.625
	1e-15- 1e-7	Kzz	4.70E-10	4.64E-10	1.277

Table 4. 3: Anisotropic Case with Kxy=0: Comparison of permeability values supplied to LIMS with those predicted from the numerical experimental data

Numerical experiment	Initial search range (L- U), m^2	Permeability	Values supplied to LIMS, m^2	Predicted value m^2	Relative error (%)
1	1e-15- 1e-9	Kxx	6.00E-10	6.00E-10	0.023
	1e-13 - 1e-7	Kyy	2.00E-10	2.00E-10	0.203
	1e-15- 1e-7	Kzz	3.00E-12	2.98E-12	0.541
		Kxy	0.00		
2	1e-12- 1e-9	Kxx	2.40E-10	2.40E-10	0.201
	1e-12 - 1e-9	Kyy	6.40E-10	6.39E-10	0.114
	1e-13 - 1e-10	Kzz	3.60E-12	3.60E-12	0.023
		Kxy	0.00		
3	1e-12- 1e-8	Kxx	4.00E-09	4.01E-09	0.217
	1e-12 - 1e-8	Kyy	4.00E-10	3.98E-11	0.301
	1e-13 - 1e-10	Kzz	9.00e-12	8.93E-12	0.734
		Kxy	0.00		

Table 4. 4: Anisotropic Case Kxy > 0: Comparison of permeability values supplied to LIMS with those predicted from the numerical experimental data, principal permeability values Kxx=8e-10, Kyy=4e-10, Kzz=2e-12 m^2

Numerical experiment	Angle of Rotation	Initial search range (L- U) m^2	Permeability	Values supplied to LIMS, m^2	Predicted value m^2	Relative error (%)
1	10	1e-12- 1e-9	Kxx	7.88E-10	7.90E-10	0.31
		1e-12 - 1e-9	Kyy	4.12E-10	4.12E-10	0.06
		1e-12 - 1e-10*	Kxy	6.84E-11	6.85E-11	0.19
		1e-14 - 1e-10	Kzz	2.00E-12	1.98E-12	1.15
2	20	1e-12- 1e-9	Kxx	7.532E-10	7.55E-10	0.21
		1e-12 - 1e-9	Kyy	4.47E-10	4.47E-10	0.05
		1e-12 - 1e-10*	Kxy	1.29E-10	1.29E-10	0.22
		1e-14 - 1e-10	Kzz	2.00E-12	1.98E-12	0.79
3	30	1e-12- 1e-9	Kxx	7.00E-10	7.00E-10	0.01
		1e-12 - 1e-9	Kyy	5.00E-10	5.00E-10	0.01
		1e-12 - 1e-10*	Kxy	1.73E-10	1.73E-10	0.01
		1e-14 - 1e-10	Kzz	2.00E-12	2.00E-12	0.02
4	40	1e-12- 1e-9	Kxx	6.347E-10	6.36E-10	0.28
		1e-12 - 1e-9	Kyy	5.65E-10	5.66E-10	0.17
		1e-12 - 1e-10*	Kxy	1.97E-10	1.98E-10	0.59
		1e-14 - 1e-10	Kzz	2.00E-12	1.98E-12	1.21
5	50	1e-12- 1e-9	Kxx	5.65E-10	5.66E-10	0.13
		1e-12 - 1e-9	Kyy	6.35E-10	6.35E-10	0.08
		1e-12 - 1e-10*	Kxy	1.97E-10	1.97E-10	0.24
		1e-14 - 1e-10	Kzz	2.00E-12	1.99E-12	0.41
6	60	1e-12- 1e-9	Kxx	5E-10	5.01E-10	0.11
		1e-12 - 1e-9	Kyy	7E-10	6.97E-10	0.48
		1e-12 - 1e-10*	Kxy	1.73E-10	1.72E-10	0.53
		1e-14 - 1e-10	Kzz	2.00E-12	2.02E-12	1.01

*the upper bounds must satisy this condition for $U_{Kxx}=U_{Kyy}=10U_{Kxy}$ and initial guess *GPY*=10*GPXY*. This is to ensure that the permeabiity is a positive definite tensor. U_{Kxx}, U_{Kyy} and U_{Kxy} are the upper limits of Kxx, Kyy,and Kxy respectively.

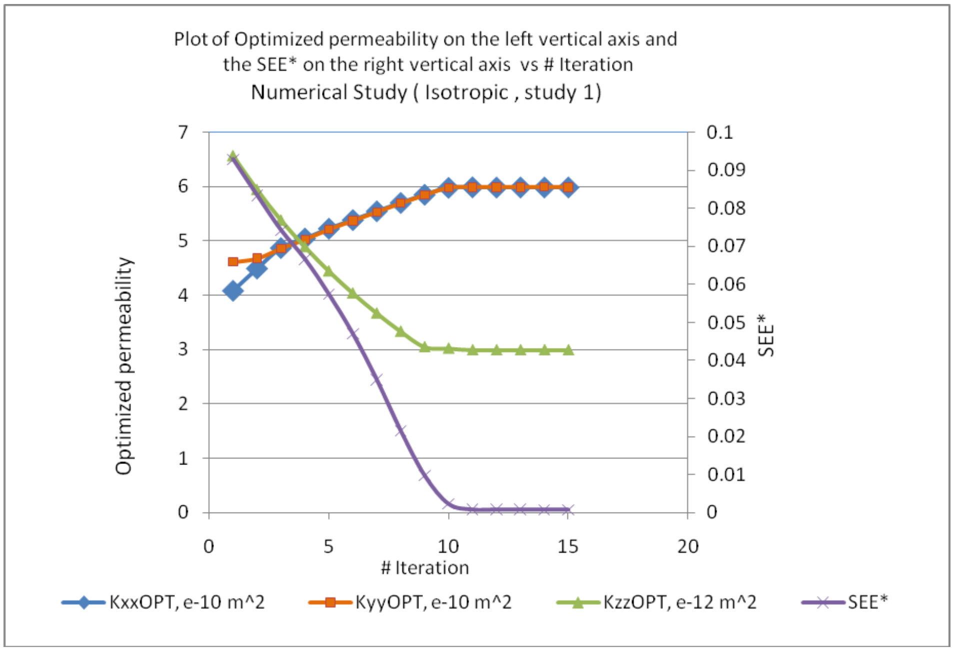

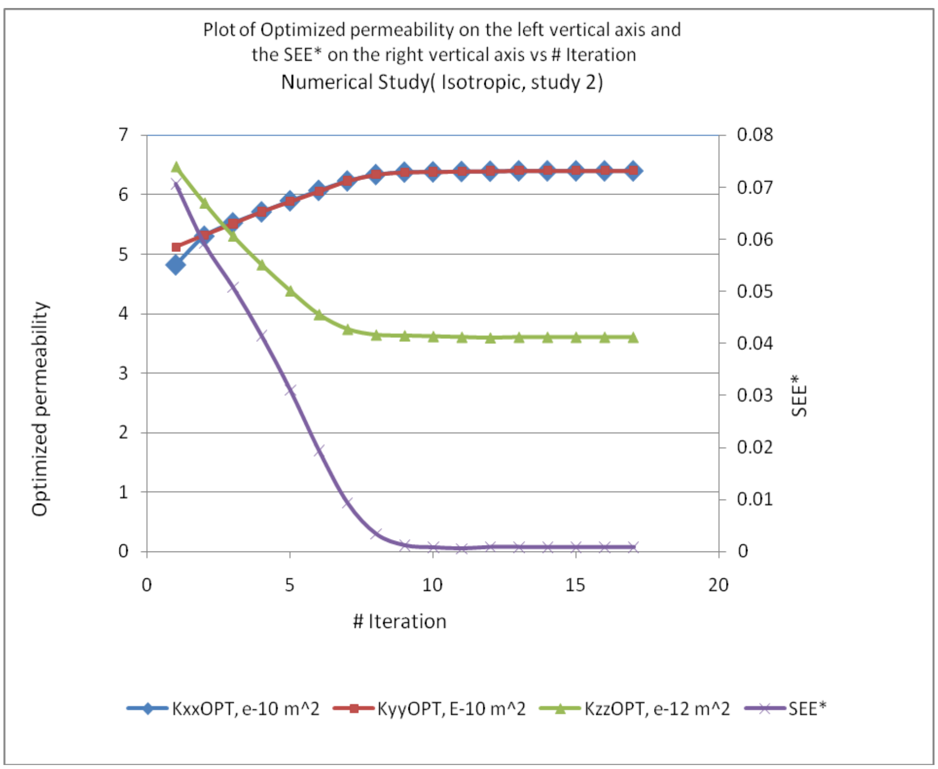

Figure 4. 2 : Numerical experimental study for transversely isotropic permeability prediction.

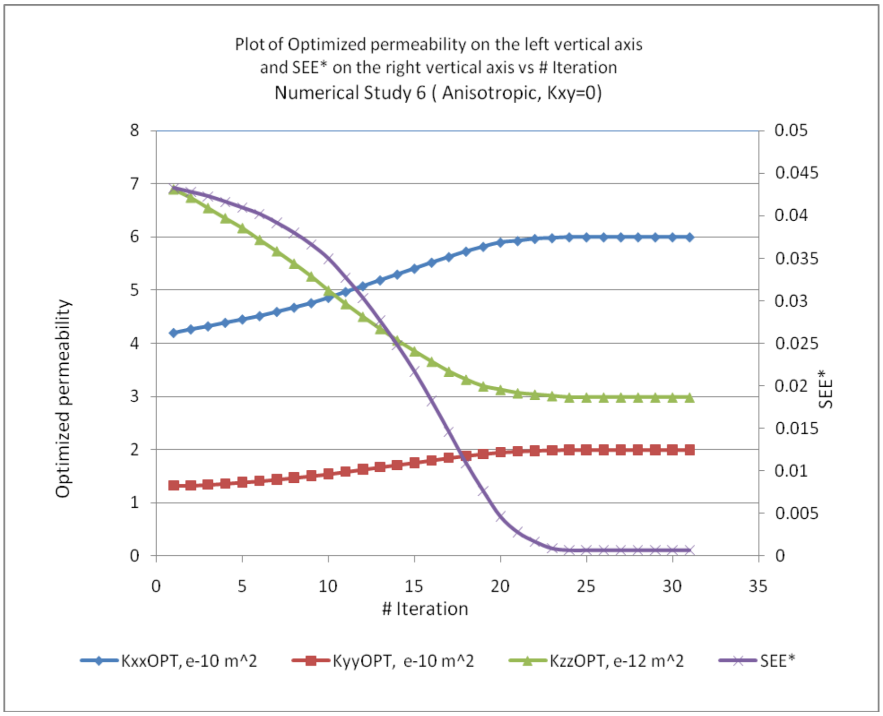

(a)

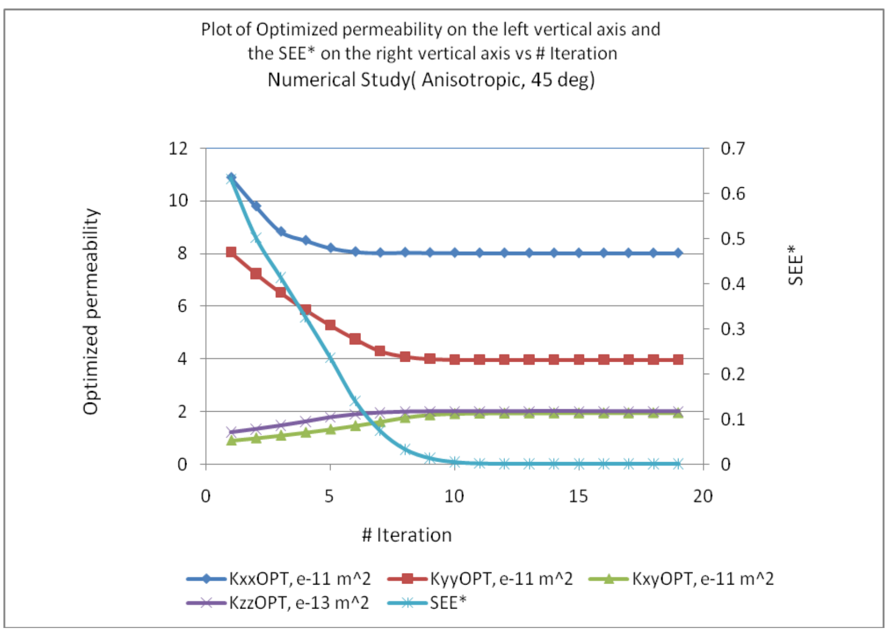

(b)

Figure 4. 3 : Numerical experimental study for transversely anisotropic permeability prediction :(a) Kxy =0 (b) Kxy > 0

The result in Figure 4.2 and 4.3 shows that the RSS value decreases and the optimized permeability values improves.

4.1.2 Distribution Media and Fabric Permeability Prediction

As shown in Figure 4.4 the tows of woven fabrics have is tendency to block the injection hole and thereby affecting the resistance to flow consequently the accurate prediction of its permeability is hampered as the numerical simulation does not assume this and hence the arrival times are being matched for conditions that are not identical. To alleviate this problem a highly permeable layer known as the distribution media (DM) can be placed over the injection hole. The effect of the placement of the distribution media on fabric permeability prediction was investigated. Four cases were considered: (1) predicting preform permeability from numerical experiment carried out with the same DM in both virtual experiment and LIMS model, (2) predicting preform permeability with DM in virtual experiment and without DM in LIMS model, (3) predicting preform permeability with DM in virtual experiment and with a different DM in LIMS model (as it may be difficult to know an exact value for DM) and (4) predicting preform permeability without DM in both virtual experiment and in LIMS model. The result in Table 4.5 shows that using the DM in the experiment and a guess of the DM permeability value in the LIMS model to find preform permeabilities does not cause much of an error. However if DM is not accounted for either in the experiment or in the model it does influence the prediction of the permeability values. The case of no DM in both the experiment and LIMS model is also ok but it is limited to non- woven fabrics. Hence the use of DM in the experiment and in LIMS model will give the most accurate and consistent preform permeability even when we do not know the exact value of permeability of the distribution media as seen from second set of results.

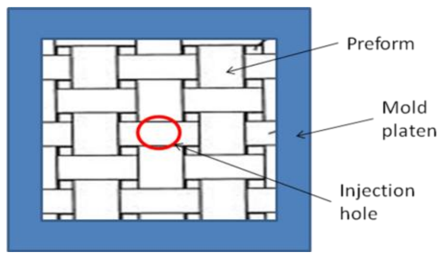

Figure 4. 4 : Bottom view of preform placed in a radial injection mold showing the injection hole being blocked by the fiber tows.

Table 4. 5: Influence of distribution media on the prediction of the three dimensional permeability of fabrics

Distribution Media(DM)			Permeability supplied to LIMS m^2			Predicted permeability m^2			DM permeability (used for optimization method)	% Relative error		
diameter (cm)	thickness (m)	permeability (virtual experiment)	Kxx	Kyy	Kzz	Kxx	Kyy	Kzz		ΔKxx	ΔKyy	ΔKzz
Case 1: DM with identical value for virtual experiment and optimization procedure to find preform permeability												
2	0.001	1.0E-08	6.0E-10	9.0E-10	4.0E-12	6.01E-10	9.02E-10	4.00E-12	1.00E-08	*0.21*	*0.21*	*0.12*
2	0.001	1.0E-09	6.0E-10	9.0E-10	4.0E-12	6.00E-10	9.01E-10	4.00E-12	1.00E-09	*0.07*	*0.09*	*0.07*
2	0.001	1.0E-10	6.0E-10	9.0E-10	4.0E-12	6.01E-10	9.02E-10	3.99E-12	1.00E-10	*0.14*	*0.20*	*0.37*
4	0.001	1.0E-08	6.0E-10	9.0E-10	4.0E-12	6.00E-10	9.01E-10	4.00E-12	1.00E-08	*0.07*	*0.10*	*0.04*
4	0.001	1.0E-09	6.0E-10	9.0E-10	4.0E-12	6.00E-10	8.99E-10	4.00E-12	1.00E-09	*0.02*	*0.07*	*0.05*
4	0.001	1.0E-10	6.0E-10	9.0E-10	4.0E-12	6.01E-10	9.01E-10	3.99E-12	1.00E-10	*0.10*	*0.16*	*0.28*
Case 2: DM with different value for virtual experiment and optimization procedure to find preform permeability												
4	0.001	1.0E-08	6.0E-10	9.0E-10	4.0E-12	5.72E-10	8.58E-10	3.80E-12	5.00E-08	4.60	4.61	4.92
4	0.001	1.0E-08	6.0E-10	9.0E-10	4.0E-12	5.69E-10	8.54E-10	3.77E-12	1.00E-07	5.10	5.10	5.73
Case 3: DM for virtual experiment and no DM in optimization procedure to find preform permeability												
2	0.001	1.0E-08	6.0E-10	9.0E-10	4.0E-12	1.46E-09	2.18E-09	9.61E-12	-	143.6	141.9	140.25
2	0.001	1.0E-10	6.0E-10	9.0E-10	4.0E-12	6.81E-10	1.02E-09	4.52E-12	-	13.5	13.3	12.9
Case 4: No DM in both virtual experiment and optimization procedure to find preform permeability												
-	-	-	6.0E-10	9.0E-10	4.0E-12	5.99E-10	9.00E-10	4.00E-12	-	0.10	0.05	0.04

4.1.3 Data Sensitivity

The sensitivity of the program to random variation in the flow arrival time was investigated. Numerical experiment was carried out for a set of permeability tensor and the flow front arrival times were subjected to some random changes Table 4.6 shows the result of the study. The results show that the program is not sensitive to random effect up to ±10% changes in the flow arrival time. And in essence within ±10% changes in the flow arrival time there is no significant changes in permeability tensor.

Table 4. 6: Sensitivity study of the permeability values (K_{xx}=8e-10, K_{yy}=4e-10, K_{xy}=0, K_{zz}=2e-12 m^2) supplied to LIMS with those predicted by the algorithm.

	PREDICTED			RELATIVE ERROR (%)		
PERTURBATION	Kxx'OPT	Kyy'OPT	Kzz'OPT	Δkxx	Δkyy	Δkzz
(± 10 % uniform distribution)	7.8260E-10	4.0852E-10	1.9993E-12	2.1746	2.129	0.0365
(± 10 % uniform distribution)	8.0614E-10	3.9559E-10	1.9940E-12	0.7669	1.1018	0.2985
(± 10 % uniform distribution)	8.0694E-10	3.9429E-10	2.0155E-12	0.868	1.4268	0.776
(± 6 % uniform distribution)	8.0642E-10	4.0095E-10	1.9951E-12	0.802	0.2372	0.2435
(± 6 % uniform distribution)	7.9836E-10	4.0401E-10	2.0029E-12	0.2046	1.0033	0.1445
(± 6 % uniform distribution)	7.9657E-10	4.0523E-10	2.0094E-12	0.4289	1.308	0.4685
(± 4 % uniform distribution)	8.0319E-10	4.0042E-10	1.9951E-12	0.399	0.1043	0.2435
(± 4 % uniform distribution)	7.9613E-10	4.0264E-10	1.9951E-12	0.4833	0.6587	0.2435
(± 4 % uniform permeability)	8.0177E-10	3.9903E-10	1.9951E-12	0.2212	0.2428	0.2435
(+ 200 % uniform distribution)	5.68E-10	2.29E-10	1.33E-12	29.0219	42.7385	33.3560
(+ 200 % uniform distribution)	5.27E-10	2.32E-10	1.35E-12	34.1211	42.0430	32.3925
(+ 200 % uniform distribution)	5.02E-10	2.48E-10	1.33E-12	37.3031	37.9530	33.3560

PERTUBATION	Average relative error (%)		
	Δkxx	Δkyy	Δkzz
(± 10 % uniform distribution)	1.2698	1.5525	0.3703
(± 6 % uniform distribution)	0.4785	0.8495	0.2855
(± 4 % uniform distribution)	0.3678	0.3353	0.2435
(+ 200 % uniform distribution)	33.4820	40.9115	33.0348

4.1.4 Global Minimum

In the approach presented here both local and global minimum can occur in the optimization which is a case of multimodal minima. In almost all instances, finding the global minimum of residual sum of squares, *RSS* for a given permeability set (Kxx, Kyy, Kzz) is of interest. The global minimum will ensure the uniqueness of the optimized permeability values obtained by the program proposed. The program is written in such a way as to find the global minimum.

And to verify that the program predicts permeability at the global minimum an experiment was carried out . The experiment was carried with one set of permeability value as in Table 4.7. The flow arrival times at the sensors were recorded using the program to predict the actual permeability values (Table 4.7). The convergence *RSS* was also recorded. Using different set of permeability values in the domain shown in Figure 4.5 the RSS between their flow arrival times and that of the experiment were obtained for each set. Each RSS including the convergence RSS is a node in the domain (1000 nodes) defined by the corresponding permeability set. Each node in the interior of the domain and at the boundary was compared with 26 nodes in its neighborhood (Figure 4.5). The convergence RSS= 2.165 is the least and the only RSS that is less than all its 26 surrounding RSS values while all other nodes within the domain of consideration have at least one node in its neighborhood with RSS value less . These two conditions satisfy the requirements for Global minimum.

Table 4. 7: Permeability values supplied to LIMS and predicted permeability values for global minimum verification

Permeability	Values supplied to LIMS, m^2	Predicted Values, m^2	%Permeability Relative Error	RSS
Kxx	6.00E-10	6.01E-10	0.17	
Kyy	9.00E-10	9.02E-10	0.22	
Kzz	4.00E-12	3.99E-12	0.25	
				2.165

A surface plot of time residual sum of square with permeability was made for ten sliced surfaces along the K_{zz} permeability axis (Figure 4.7). The two *RSS* extreme surfaces, *S1* and *S5* are shown in Figure 4.7. The *RSS* global minimum is on surface *S5* which corresponds to the optimized or predicted permeability set shown in Table 4.7. And it shows that the predicted permeability values are obtained at the global and not at a local minimum. Hence the program will always seek and predict the correct permeability values corresponding to the global minimum, *RSS*.

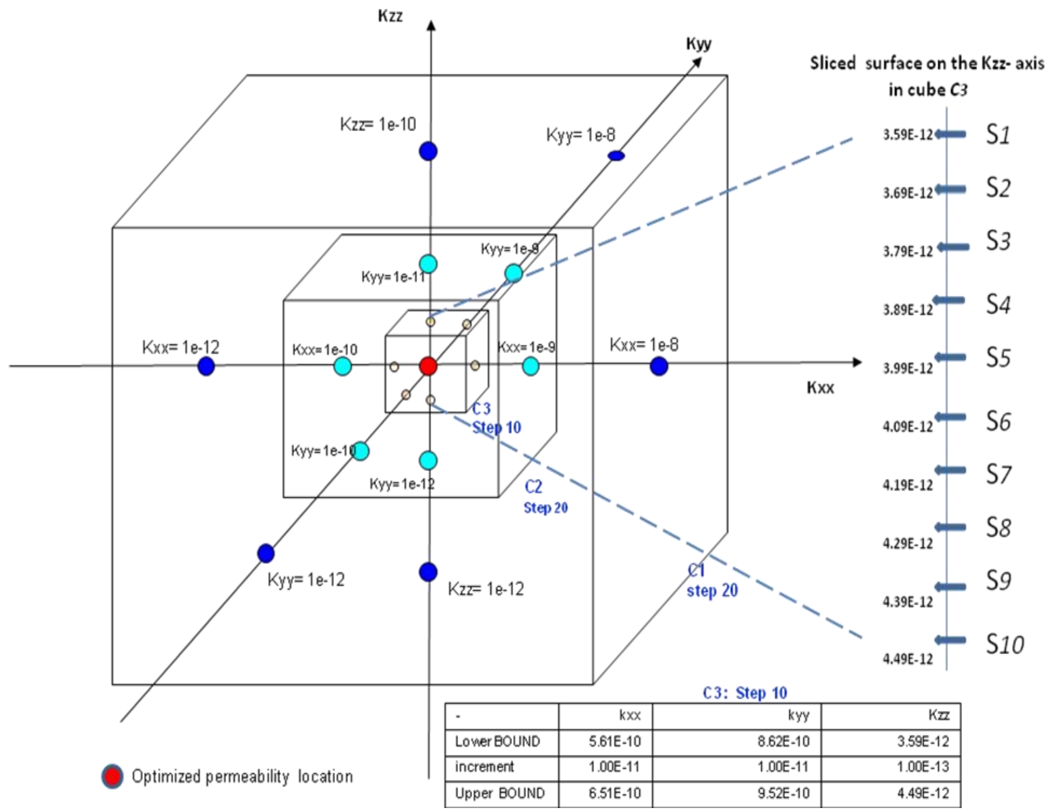

-	kxx	kyy	Kzz
Lower BOUND	5.61E-10	8.62E-10	3.59E-12
increment	1.00E-11	1.00E-11	1.00E-13
Upper BOUND	6.51E-10	9.52E-10	4.49E-12

Figure 4. 5: Global minimum verification domain. The domain includes the upper and lower bounds for Kxx, Kyy, Kzz used in the optimization

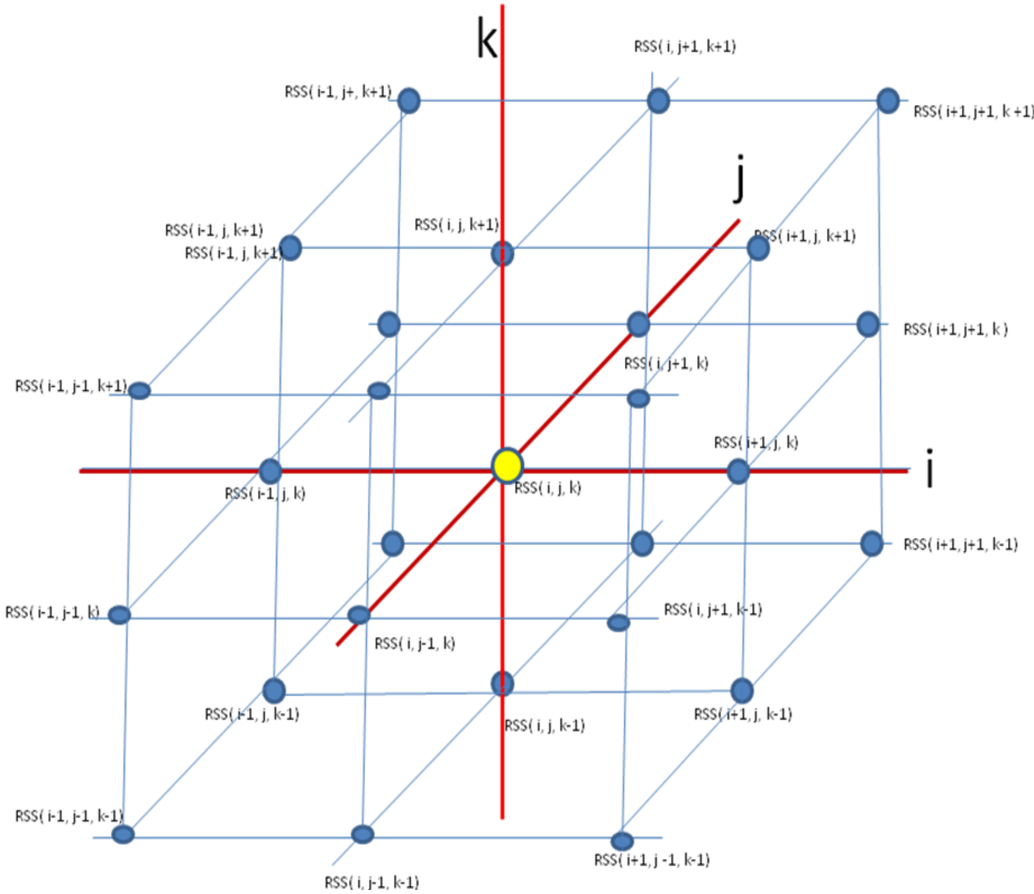

Figure 4. 6 : RSS global minimum verification cube.

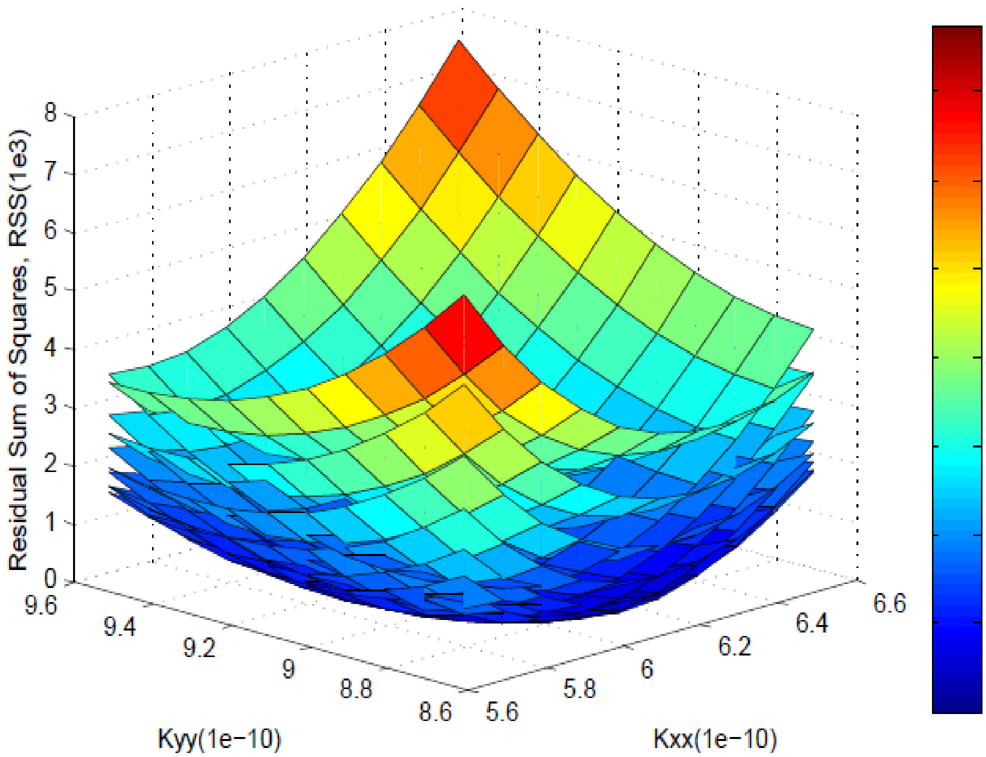

Figure 4. 7 : Ten surface plot of time residual sum of squares with permeability

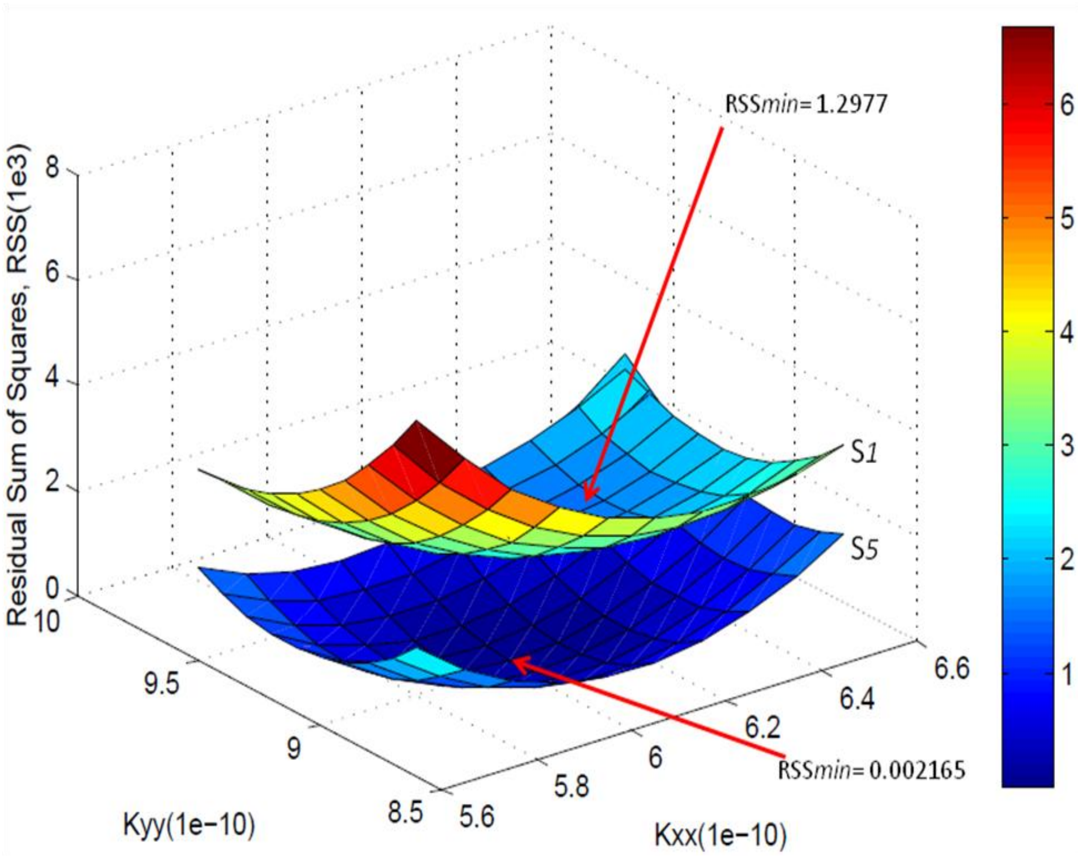

Figure 4. 8: Surface plot of extreme time residual sum of squares with permeability

4.1.5 Limitations

The approach is limited to fabrics with Kxx/Kyy less than 11 because of the arrangement of the sensors in the experimental set-up. The resin will reach the last sensor in the x direction before it can wet 1 or 2 sensors in the yy direction. This is not that limiting as even for unidirectional fabric, the kxx to kyy ratio is less than 10. Also one could make sure that the principle directions are not aligned with the x and y directions thus allowing for Kxy to be not zero and thus reduce the kxx/kyy ratio.

And the experimental set-up can only be used for non-carbon fibrous media in its current state though this might be alleviated by using a glass fabric veils or different sensors. Figure 4.9 show the limit of fabric anisotropy that can be determined with the experimental set-up.

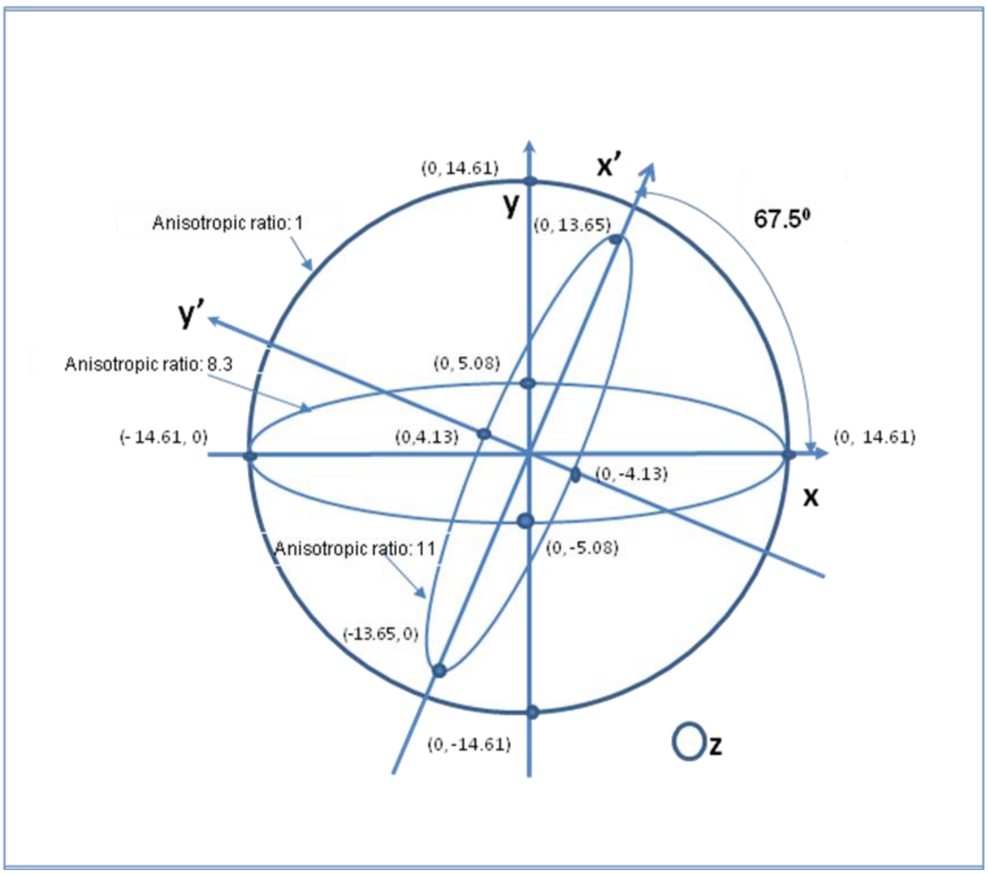

Figure 4. 9: Experiment set-up limit of fabric in-plane anisotropy

4.2 Experimental

4.2.1 Design of Experiments

In order to verify the described procedure for permeability tensor prediction a number of 3D mold filling experiments were carried out. The experiments were conducted by injecting corn syrup through a small hole on the bottom plate at constant pressure.

The injection pressure, P_i, was measured using pressure gauges mounted on the pressurized paint tank and the viscosity, μ, of the corn syrup was measured using viscometer (Brookfield DV-E Viscometer) before the experiment. A total of n layers of preform stacked on top of each other resulted in a fiber volume fraction, v_f , when compressed to stack thickness, h, using the hydraulic press.

The experiment was carried out for Scotchbrite pad manufactured by 3M. The fabric was chosen based on smaller density variations than continuous-strand mat and ease of handling. Woven and stitched LCM preforms were avoided due to their tendency to have variation in fabric architecture. Proper preform handling is a key to obtaining consistent experimental results. Other factors that might affect the experimental results are fluid viscosity, and preform density (brings about permeability variations).

Table 4. 8: Parameters for point injection experiments

Parameter	Preform
	Scotchbrite
Dimensions (compressed)	30x30x0.6 cm
Number of layers , n	2
Fiber volume fraction, v_f , (%)	20
Viscosity μ ,Pas	0.1
Injection pressure P_i ,Pa	$1x10^5$

4.2.2 Processing of Experimental Data

The data acquisition system was stopped when any of the outer most sensors was triggered this is to ensure the accuracy of the flow front arrival time. After each experiment the flow front arrival times were stored in csv file and the preform was taken out from the mold. And the flow front $Aspect\,ratio = a'/b'$ was measured and recorded as shown in Figure 4.9. This was used to compare with the aspect ratio of the predicted permeability since it is the squared root of the ratio of the in-plane permeability values. The flow front arrival times are then supplied to the program as shown in Figure 3.8 for permeability prediction.

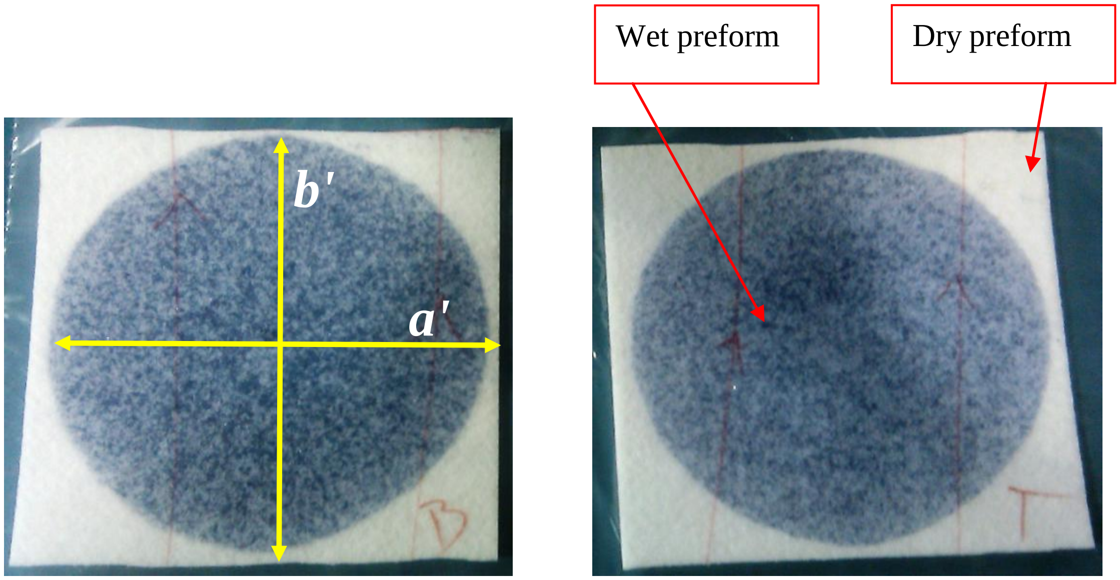

(a) (b)

Figure 4. 10: Snapshots of the flow front at the end of the experiment. The measurement *a' and b'* are used to calculate the aspect ratio (a) bottom layer (b) top layer

4.2.3 Experimental Results and Flow Front Comparison

The permeability results from five experiments are presented in Table 4.9 These experiments were completed using two layers of Scotchbrite and using 6mm spacers. The injection pressure and viscosity are constant in all five cases. The experimental flow front at time, t=22, 28, 34s, were plotted and compared with that of the predicted permeability. Figure 4.11 – 4.13 presents the flow-front comparisons for *SB3* at 22, 28 and 34 s respectively.

Table 4. 9: Scotchbrite predicted permeability data

	Predicted permeability, m^2			Aspect ratio	
				LIMS (predicted)	Experiment
Experiment, *N*	Kxx	Kyy	Kzz	a/b	a'/b'
SB1	2.12E-09	2.35E-09	4.58E-10	0.95	0.97
SB2	2.84E-09	3.00E-09	4.73E-10	0.97	1.02
SB3	2.75E-09	2.98E-09	5.72E-10	0.96	0.98
SB4	2.43E-09	2.65E-09	4.62E-10	0.96	0.99
SB5	2.35E-09	2.65E-09	5.50E-10	0.94	0.97

Using the expression given in [71] for mean, standard division and precision limit:

$$\bar{k} = \frac{1}{N}\sum_{i=1}^{N} k_i \tag{4.1}$$

$$S_k = \left[\frac{1}{N-1}\sum_{i=1}^{N}(k_i - \bar{k})^2\right]^{1/2} \tag{4.2}$$

$$P_k = tS_k \tag{4.3}$$

Where t = 2.77645, from table A.2, Student's t Table, in ref. [71]. The average permeability values with 95% confidence interval and bias errors neglected are given in Table 4.10.

Table 4. 10: 95% confidence interval for Scotchbrite **permeability values**

Statistical measure	Kxx, m^2	Kyy, m^2	Kzz, m^2
Mean	2.50E-09	2.73E-09	5.03E-10
SD	0.29E-09	0.27E-09	0.54E-10
95% confidence interval	(2.50±0.82)E-9	(2.73±0.75)E-9	(5.03±1.50)E-10

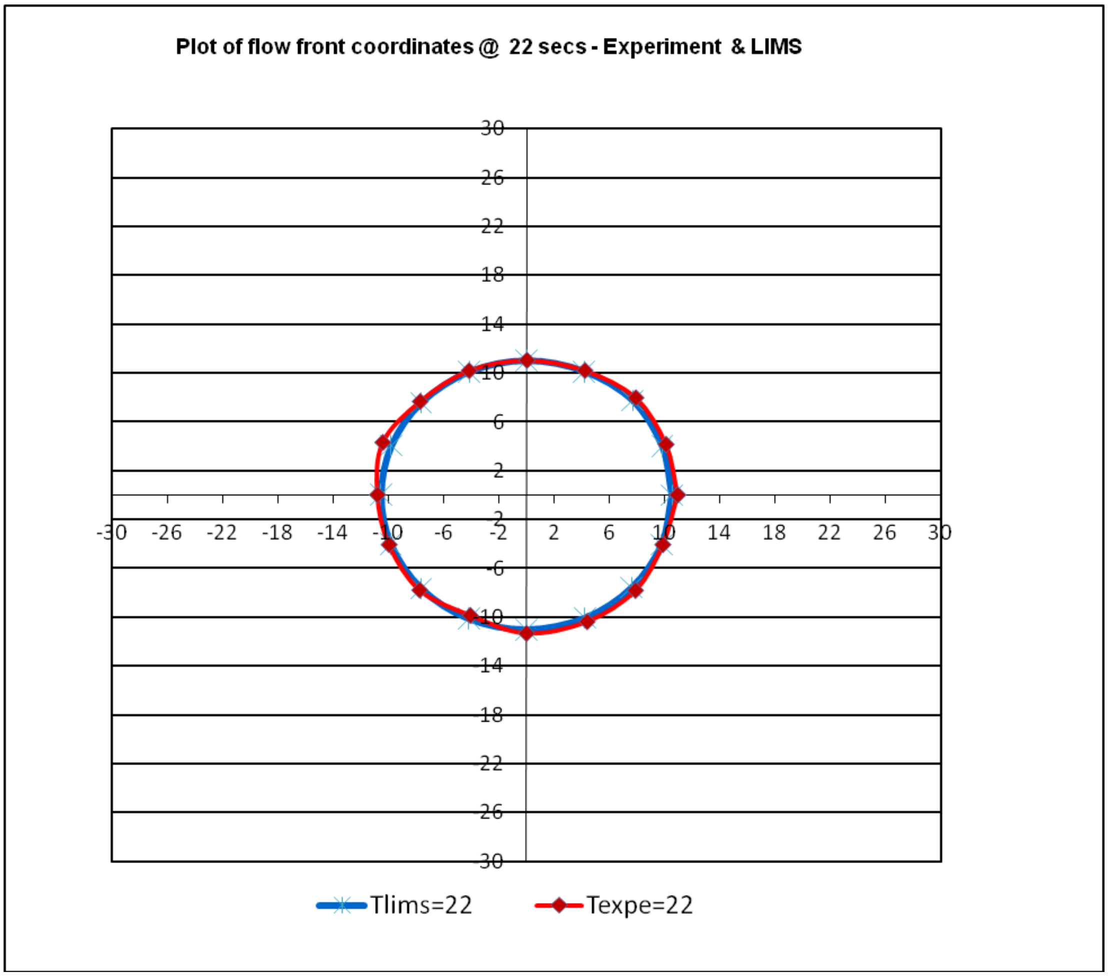

Figure 4. 11: Superimposed experimental and LIMS model flow front comparison for *SB3* at 22 s

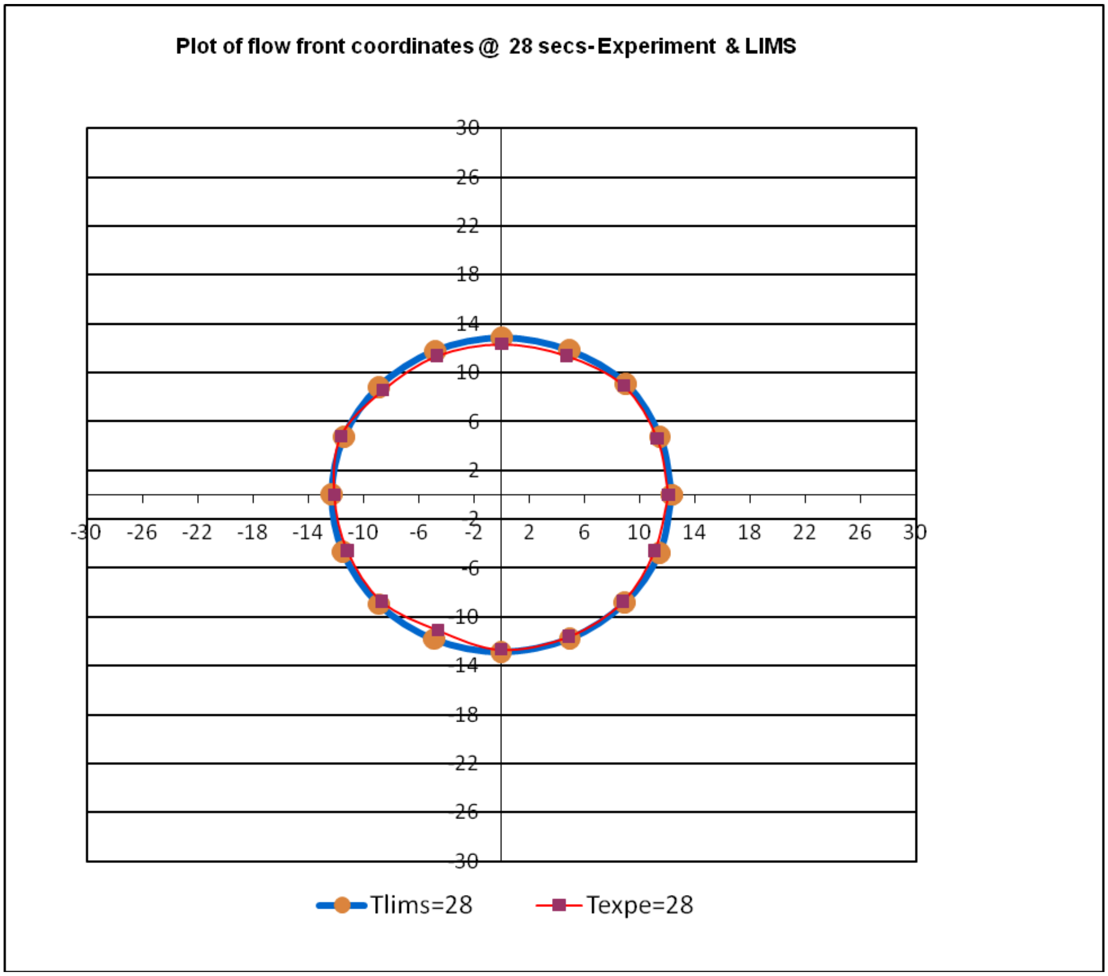

Figure 4. 12 : Superimposed experimental and LIMS model flow front comparison for *SB3* at 28s.

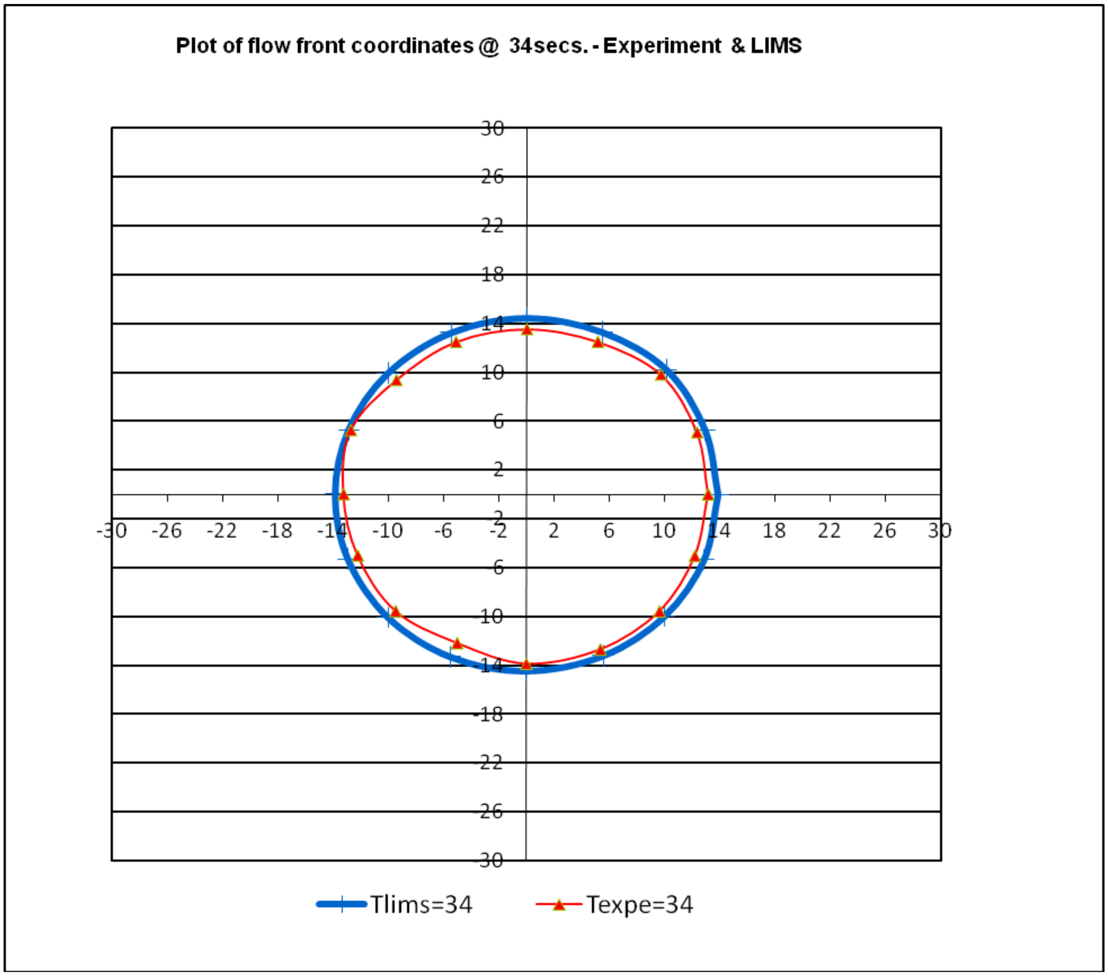

Figure 4. 13: Superimposed experimental and LIMS model flow front comparison for *SB3* at 34 s. Bickerton obtained mean bulk permeability values at 8.3 and 11.9 % fiber volume fraction as 4.19e-9 and 1.21e-9 m^2.

4.3 Conclusions

The following conclusions can be drawn from this chapter

- The numerical experimental and permeability prediction results shows that predict results shows that the permeability of fabrics can be predicted by matching simulated flow front arrival times with that of experimental flow front arrival times.

- Placing distribution media over the injection hole on the experimental set-up and using DM in the LIMS model will enhances the accurate prediction of fabric three dimensional permeability values.

- Figure 4.11- 4.13 confirms that the predicted permeability flow front matches that of the experiment. And that the new approach predicts permeability values at the global minimum.

- The proposed approach can be used to determine three-dimensional permeability of fibrous reinforcements used in composite materials without the use of any preform embedded sensors, optical imaging and X-ray spectroscopy.

Chapter 5

SUMMARY, CONTRIBUTIONS AND FUTURE WORK

5.1 Summary and Contributions

A mixed experimental/numerical technique for the prediction of 3D permeability tensor of fabrics was proposed. The technique is based on an existing experimental set-up and which records resin arrival time at an array of locations in experimental mold. Numerical optimization of the least-squares error between the experimental data and data predicted with variable permeability values from RTM simulation is then performed to obtain the actual values of permeability components. Serial application of golden section search optimization technique was used to perform the optimization adjusting the parameters in a finite element model of the experiment to optimize the agreement between measured and calculated flow front arrival times. As implemented, this technique evaluates four permeability components - three in-plane and one transverse - in a single experiment. Extension to find the through-the-thickness skew components is straightforward, but large preform thickness might be needed. Currently these components are assumed to be zero, which is reasonable for most woven and stitched preforms because of the symmetry.

The sensitivity to sensor data error was evaluated. Numerical results show that the program is not sensitive to random effect up to $\pm$10% changes in the flow arrival time. And in essence within $\pm$10% changes in the flow arrival time there is no significant changes in the permeability tensor.

The advantage of this approach is that it can be used to obtain permeability values from a single experiment; there is no need to scale the circular injection inlet, and it is not limited to principal permeability values. The sensors utilized are unobtrusive to the flow unlike say optic fibers embedded in the fabric that interfere with the flow of the test fluid. The electrical resistance sensors used in this approach are embedded in mold platens instead and which flush with the surface. The method can be used to help predict and understand resin flow behavior during liquid molding of advanced composite materials.

An important finding of this work is to use a distribution media at the inlet to ensure that the inlet hole is not on top of a woven tow which will give erroneous results. When using the optimization technique, the LIMS model should also have a distribution media and it was found that if one is off by an order or two in the choice of the DM value, the results are still within acceptable ranges for the preform permeability.

The overall contributions of this work to the field of Liquid Composite Molding processes lies in the development and experimental demonstration of a new methodology to characterize the three dimensional permeability of fibrous media from one experiment.

5.2 Future Work

Some suggestions for future work are stated as below:

- Numerical study has been done as shown in Table 4.5 that distribution media can be placed over the mesh injection hole to prevent the effect of fiber tows blocking it. And instead of using distribution media circular wire gauze or mesh washer screen can be used. This can be place over the injection hole permanently in such a way that it flushes with the surface of the mold platen. This will ensure that every experiment will be subjected to the same injection treatment. However this needs to be investigated.

- Presently only 6 mm spacer thickness was investigated. Varying spacer thickness needs to be investigated. There is a need to apply the method for measuring permeability of deformed preforms - variable fiber volume fraction and shear deformation.

- The proposed method can be extended to measure all six permeability components in thick 3D woven/ braided preforms. The present work was centered on four (diagonal and one in-plane off diagonal) components.

- Situation where some of the sensors do not trigger and prior to sending the acquired flow front arrival times to LIMS these un-triggered sensors will have to be manually commented out. Speeding the computation, getting automated system to recognize errors in sensor feedback, etc. can be beneficial.

- The experimental set-up is presently limited to non-carbon fibrous media. Further study needs to be done in other to use the set-up for characterizing carbon fibers. And better system of drying the sensors after each experiment needs to be incorporated to avoid delay being experienced while waiting for the sensors to dry. Designing and building a standalone workstation for the experimental set-up is desirable.

REFERENCES

[1] Pavel, Simacek, S. and Advani, S.G., Simulations for Design, Optimization and Control of Liquid Composite Mold Filling, Cancom Talk (2) (2003)

[2] Baichen, L., Bickerton , S. and Advani, S.G., Modelling and simulation of resin transfer molding (RTM)—gate control, venting and dry spot prediction, *Composites Part A* **27A** (2) (1996), pp. 135–141.

[3] Nedanov, P.B. and Advani, S.G. (2002). A Method to Determine 3D Permeability of Fibrous Reinforcements, Journal of Composite Materials, 36(2): 241–254.

[4] Dominique, B., Øyvind, N., Luc, S., Peter, C., Permeability assessment by 3D interdendritic flow simulations on microtomography mappings of Al–Cu alloys, Materials

[5] Seeman II, W., 1990, ‘‘Plastic Transfer Molding Techniques for the Production of Fiber Reinforced Plastic Structures,’’ United States Patent 4,902,215, February

[8] Luce, T., Advani, S.G., Howard, G. and Parnas, R. (1995). Permeability Characterization: Part 2: Flow Behavior in Multiple-layer Preforms, Polymer Composites, 16(6): 446–458.

[9] Trevino, L., Rupel, K., Young, W.B., Liou, M.J. and Lee, L.J. (1991). Analysis of Resin Injection Molding in Molds with Replaced Fiber Mats. 1: Permeability and Compressibility Measurement, Polymer Composites, 12(1): 20–29.

[10] Wu, C.H., Wang, T.J. and Lee, L.J. (1994). Trans-plane Fluid Permeability Measurement and its Application in Liquid Composite Molding, Polymer Composites, 15(4): 289–298.

[11] Weiztenbock, J.R., Shenoi, R.A. and Wilson, P.A. (1998). Measurement of Three-dimensional Permeability, Composites Part A, 29(1): 159–169.

[12] Ahn, S.H., Lee, W.L. and Springer, G.S. (1995). Measurement of the Three-dimensional Permeability of Fiber Performs using Embedded Fiber Optic Sensors, Journal of Composite Materials, 29(6): 714–733.

[13] Stoven, T., Weyrauch, F., Mitschang, P. and Neitzel, M. (2003). Continuous Monitoring of Three-dimensional Resin Flow through a Fibre Perform, Composites: Part A, 34(7): 475–480.

[14] Woerdemen, D.L., Phelan, F.R. and Parnas, R.S. (1995). Interpretation of 3-D Permeability Measurements for RTM Molding, Polymer Composites, 16(6): 470–480.

[15] Markicevic, B. and Papathanasiou, T.D. (2003). A Model for the Transverse Permeability of Bi-material Layered Fibrous Performs, Polymer Composites, 24(1): 68–82.

[16] Parnas, R., Luce, T., Advani, S.G. and Howard, G. (1995). Permeability Characterization:Part 1: A Proposed Standard Reference Fabric for Permeability, Polymer Composites, 16(6): 429–445.

[17] Drapier, S., Pagot, A., Vautrin, A. and Henrat, P. (2002). Influence of the Stitching Density on the Transverse Permeability of Non-crimped New Concept (NC2) Multiaxial Reinforcements: Measurements and Predictions, Composites Science and Technology, 62(15): 1979–1991.

[18] Henry, D., *Les Fontaines Publiques de la Ville de Dijon* ("The Public Fountains of the Town of Dijon"), Dalmont, Paris (1856).

[19] Liakopoulos, A., On the tensor concept of the hydraulic conductivity, Rev. Engineering, Am. Univ. Beirut, no. 4. 35-42, October 1961

[20] Liakopoulos , A., Variation of the Permeability Tensor Ellipsoid in Homogeneous Anisotropic Soils, Water Resources Research, 1 (1) (1965), pp. 135-141

[21] Ene, H.I., and Polisevski, D., Thermal Flow in Porous Media , D. Reidel , Dordrect,(1987)

[22] E. Sanchez-Palencia, E. and Zaoui, A. ed., Homogenization Techniques for Composite Media. Lecture Notes in Physics Vol. 272, Springer , Berlin(1987)

[23] Chang, W. ; Kikuchi,N. ; Analysis of non-isothermal mold filling process in resin transfer molding (RTM) and structural reaction injection molding (SRIM), Computaional Mechanics, 16 (1), (1995).

[24] Dimitrovova,Z. and Faria, L.; Finite element modeling of resin transfer molding process based on homogenization techniques , Computers and Structures, 76(1), (2000).

[25] Koponen, A., Kataja M., and Timonen J., 1997 , Permeability and effective porosity of porous media, Physical Review E., 56(3), 1997.

[26] Koponen, A., Kandhai, D., Hellen, E., Alava, M., Hoekstra, A.,Kataja M., Niskanen, K., Sloot, P., and Timonen J., 1997 , Permeability of three-dimensional random fiber webs,. , Physical Review Letters, 80(4), 1997.

[27] Nabovati, A., Sousa, A.C.M., LBM mesoscale modeling of porous media, *Int Rev Mech Eng* **2** (4), 2008.

[27] Nabovati, A., Llewellin, E.W., Sousa , A.C.M., A general model for the permeability of fibrous porous media based on fluid flow simulations using the lattice Boltzmann method, Composites Part A: Applied Science and Manufacturing 40(6-7),2009, :860-869

[29] Gauvin, R., Kerachi, A. and Fisa, B., Variation of Mat Surface Density and Its Effects on Permeability Evalaution for RTM Modeling, Journal of Reinforced Plastics,13,(1994)

[30] Gebert,B.R., Permeability of Unidirectonal Reinforcements for RTM, Journal of Composite Materials, 26(8) (1992): 1100-1133

[31] Simacek ,P., an S.G. Advani, permeability Model for a Woven Fabric, Polimer Composites 17,(1996).

[32] Parnas, R. S., and Salem, A.J., A Comparison of the Unidirectional and Radial In-Plane Flow of Fluids Through Woven Composite Renfoncements , Polymer Composites, 14(5), (1993).

[33] Kim, Y.R., McCathy, S.P., Fanucci, J.P., Nolet, S.C., and Koppernaes , C., Resin Flow through Fiber Reinforcements during Composite Processing : 22nd International SAMPE Technical Conference, (1990).

[34] Bensoussan, A., Lions, J.L., and Papanicolau, G., Asymptotic Analysis for Periodic Structures, North- Holland, Amsterdam, (1978)

[35] Dave, R.C., and Kardos , J.L., and Dudocovic, M.P., A Model for Resin Flow during composite processing. Part 2: Numerical Analysis for Unidirectional Graphiate/ Epoxy Laminates , Polymers Composites , 8(2), (1987).

[36] Lam, R.C., and Kardos, J.L., The permeability and compressibility of Aligned and Cross-plied Carbon Fiber Beds during Processing of Composites

[37] S.G Advani , M.V. Buschke and R. Parnas, Chapter 12 : Resin Transfer Molding , pp. 465-516 in flow and Rheology in polymeric Composites Manufacturing , Edited by Suresh G. Advani, Elsevier Publishers, Amsterdam (1994)

[38] M. Kaviany, Principles of heat transfer in porous media (2nd ed.), Springer, New York (1995).

[39] Peng Xu and Boming Yu**,** Advances in Water Resources Volume 31, Issue 1, January 2008, Pages 74-81, Developing a new form of permeability and Kozeny–Carman constant for homogeneous porous media by means of fractal geometry

[40] Gutowski, T.G., Cai, Z., Boucher, D.,Kingery, J., Winman, S., Consolidation Experiemnts for Laminate Composites, Journal of Composite Materials, 21(7), (1987)

[41] Skartsis,, R.C., and Kardos , J.L., The Newtonian permeability and consolidation of oriented carbon fiber beds , Proceedings of the American Society for Composites Fifth Technical Congference, (1990)

[42] Chiemlewski, S., Petty, C.A, Jayaraman, K., Crossflow Permeation of Viscous and Viscoelastic Liquids in Cylinders Arrays, Processings of the Sociiety for Composites Fith Technaical Conference (1990).

[43] Buschke ,M.V. , A Predictive Model for Permeability and Non-Isothermal Flow of Viscous and Fluids in anisotropic fibrous media , PhD thesis, University of Delaware, Newark, (1992).

[44] Song, Y.S. and Youn, J.R.., Asymptotic expansion homogenization of permeability tensor for plain woven fabrics , Composites Part A: Applied Science and Manufacturing ,Volume 37, Issue 11, November 2006, Pages 2080-2087

[45**]** E. B. Belov , S. V. Lomov', Ignaas Verpoest , T. Peters , D. Roose , R. S. Parnas , K. Hoes and H. Sol **,** Modelling of permeability of textile reinforcements: lattice Boltzmann method,Composites Science and Technology 64(7-8),2004, :1069-1080

[46] Koponen, A., Kataja M., and Timonen J., 1997 , Permeability and effective porosity of porous media, Physical Review E., 56(3), 1997.

[47] Cancelliere, A., Chang , C., Foti, E., Rotherman, D.H. and Succi, S. The permeability of a random medium: Comparison of simulation with and theory. Physics of Fluids A, 2, (1990)

[48] Kohring , G.A., Calculations of the Permeability of porous media using hydrodynamic cellular automata, Journal of Statistical Physics , 63,(1991).

[49] Maier, R.S. , Kroll, D.M., Davis , H.T., and Bernard , R.S., Pore scale flow and dispersion , International Journal of Modern Physics C, 9(8), (1998).

[50] Bosl , W.J., Dvorkin, J., and Nur, A., A study of porosity and permability using Lattice- Boltzmann simulation , Geophysical Research Letters , 25(9)

[51] Papthanasiou,T.D., On the effective permeability of square arrays of permeable fiber tows , international Journal of Multiphase Flow 23, (1997).

[52] Phelan, F.R. and Wise, G., Analysis of Transverse Flow in Aligned fibrous porous media, Composite Part A, 27A(1),(1996)

[53] Berny, C.A., Permeability of Woven reinforcements for resin transfer molding, M.Sc. thesis , Univeristy of Illinois at Urbana –Champaign(1993)

[54] Kim, Y.R., McCathy, S.P., Fanucci, J.P., Nolet, S.C., and Koppernaes , C., Resin Flow through Fiber Reinforcements during Composite Processing : 22nd International SAMPE Technical Conference, (1990).

[55] Belov**,** E. B., Lomov, S. V., Verposet, I., Peters,T., Roose,D., Parnas **,**R. S., Hoes, K. and H. Sol**,** Modelling of permeability of textile reinforcements: lattice Boltzmann method, Composites Science and Technology Volume 64, Issues 7-8, June 2004, Pages 1069-1080

[56] Hoes, K., Dinescu, D., Sol, H., Vanheule, M., Parnas, R.S., Luo, Y., and Verpoest, I.**,** New set-up for measurement of permeability properties of fibrous reinforcements for RTM , Composites Part A: Applied Science and Manufacturing Volume 33, Issue 7, 1 July 2002, Pages 959-969

[57] Sun K.K, and Isaac M. D., Determination of three-dimensional permeability of fiber preforms by the inverse parameter estimation technique, Composites Part A: Applied Science and Manufacturing Volume 34, Issue 5, May 2003, Pages 421-429

[58] Adams, K. L., Miller, B., and Rebenfield, L., Forced In-Plane Flow of Epoxy Resin in Fibrous Networks, Polymer Engineering and Science , 26(20), (1986)

[59] Chan, A. W., Hwang , S.T., Anisotropic in-plane permeability of fabric media, Polym Eng Sci 1991 ; 31(16) :1233-9

[60] Gebert , B.R., and Lidstrom, P., Measuremnt of In-Plane Permeability of Anisotropic Fiber Reinforcements , Polymer Composites, 17(1),(1996)

[61] Lundstrom, T.S., Stenberg, R., Bergstrom, R., Partanen, H., Birkeland, P.A., In-Plane Permerability Measurement : a Nordic Round-Robin Study, Composite : Part A, 31,(2000)

[62] Lekakou, C., Johari, M.A.K. , Norman, D. and Bader , M.G., Measurement Techniques and Effects on In-Plane Permeability of Woven Cloths in Resin Transfer Moulding , Composites : Part A, 27A,(1996)

[63] Chae, H.S., Song, Y.S., and Young, J.R., Transverse permeability measurement of a circular braided preform in liquid composite molding, Korea-Australia Rheology Journal Vol. 19, No. 1, March 2007 pp. 17-25

[64] Gokce**,** A., Chohra, M., Advani, S.G., and Walsh, S.M., Permeability estimation algorithm to simultaneously characterize the distribution media and the fabric preform in vacuum assisted resin transfer molding process, Composite Science and Technology 65(2005), 2129- 2139.

[65] A. Saouab , J. BreÂard , P. Lory , B. Gardarein , G. Bouquet , Injection simulations of thick composite parts manufactured by the RTM process, Composites Science and Technology 61 (2001) 445-451

[66] Liu, Q., Giffard, H.S., and Parnas, R.S. New set-up for in-plane permeability measurement. Composites: Part A, 38:954–962, 2007.

[67] Simacek, P., Ledermann, C., and Advani, S. G., 2001, ‘‘Fast Three Dimensional Numerical Simulation of Isothermal Mold Filling for Liquid Composite Molding Processes,’’ *Proceedings of the American Society for Composites Sixteenth Technical Conference*, September 9–12.

[68] Advani, S. G., and Simacek, P., 1999, ‘‘Modeling and Simulation of Flow,

Heat Transfer and Cure,'' in *Resin Transfer Molding For Aerospace Structures*, Edited by T. Teresa Krukenberg and R. Paton, Kluwer Academic Publishers, Netherlands, pp. 225–281

[69] Steven,C.C., and Raymond P.C., Numerical methods for engineers , McGraw-Hill, 6 ed., 2010, 352- 353.

[70] Simacek, P., and Advani, S.G., Desirable Features in Mold Filling Simulations for Liquid Composite Molding Processes, Polymer Composites**,** Volume 25, Issue 4 (p 355-367)**,** 2004

[71] Colman, H. W. , and Steele , W.G.Jr., Experimentation and uncertainty analysis for engineers , John Wiley and Sons(1989)

APPENDIX A

SCOTCHBRITE EXPERIMENTAL DATA

Sensor #	Radial Distance(cm)	Radial line angle (radian)	Flow arrival time Experiment 1 (s)	Flow arrival time Experiment 2 (s)	Flow arrival time Experiment 3 (s)	Flow arrival time Experiment 4 (s)	Flow arrival time Experiment 5 (s)
1	5.08	0	3.828	4.531	3.625	5.141	3.328
2	6.99	0	8.234	8.531	7.75	9.437	7.422
3	8.89	0	14.328	13.937	13.25	15.328	13.828
4	10.8	0	23.531	21.437	20.953	23.828	22.828
5	12.7	0	35.437	31.734	30.656	34.531	35.422
6	14.61	0	0	0	0	0	0
7	4.13	0.39	2.234	3.125	2.219	3.531	2.016
8	6.03	0.39	6.031	6.531	5.641	6.828	5.328
9	7.94	0.39	11.734	11.437	10.859	11.734	10.828
10	9.84	0.39	19.328	18.031	17.953	18.531	18.219
11	11.75	0.39	29.828	26.531	26.156	27.828	27.922
12	13.65	0.39	43.641	39.531	36.859	40.141	42.719
13	5.08	0.79	3.828	4.625	3.734	4.828	3.625
14	6.99	0.79	8.328	8.437	7.953	8.734	7.516
15	8.89	0.79	14.828	14.031	13.359	14.234	14.125
16	10.8	0.79	23.828	22.031	20.75	21.641	23.516
17	12.7	0.79	35.641	31.437	29.859	31.328	35.016
18	14.61	0.79	0	0	41.781	45.734	0
19	4.13	1.18	2.234	3.125	2.219	3.328	2.016
20	6.03	1.18	5.625	6.031	5.531	6.531	5.219
21	7.94	1.18	11.328	10.828	10.562	11.234	10.516
22	9.84	1.18	18.734	17.234	16.859	17.641	17.625
23	11.75	1.18	29.125	25.531	25.156	26.734	28.328
24	13.65	1.18	0	0	0	0	0
25	5.08	1.57	3.734	4.234	3.625	4.734	3.219
26	6.99	1.57	8.125	7.937	7.547	8.641	7.219
27	8.89	1.57	14.234	13.328	13.25	14.234	13.016
28	10.8	1.57	23.031	20.531	20.75	21.937	21.922
29	12.7	1.57	48.344	44.328	41.578	46.031	0

30	14.61	1.57	48.344	44.328	41.578	46.031	0
31	4.13	1.96	2.234	3.031	2.219	3.328	1.828
32	6.03	1.96	5.531	6.031	5.531	6.531	4.828
33	7.94	1.96	11.031	10.625	10.359	11.328	9.719
34	9.84	1.96	18.328	16.437	16.953	18.031	16.828
35	11.75	1.96	28.937	25.328	24.859	27.234	27.219
36	13.65	1.96	42.344	36.531	35.859	39.234	42.016
37	5.08	2.36	3.828	4.625	3.734	4.828	3.219
38	6.99	2.36	8.125	8.234	7.844	8.937	7.125
39	8.89	2.36	14.625	13.531	13.359	14.531	12.625
40	10.8	2.36	23.531	20.531	21.25	22.328	20.922
41	12.7	2.36	35.844	30.125	30.859	32.031	32.125
42	14.61	2.36	0	0	0	0	0
43	4.13	2.75	2.328	3.234	2.328	3.531	1.922
44	6.03	2.75	6.125	6.437	5.641	6.828	4.828
45	7.94	2.75	0	0	0	0	0
46	9.84	2.75	19.531	16.828	17.062	18.234	16.219
47	11.75	2.75	29.937	0	0	27.328	25.719
48	13.65	2.75	44.234	38.031	37.172	40.328	40.219
49	5.08	3.14	4.234	4.734	3.828	4.937	3.125
50	6.99	3.14	8.937	8.625	7.953	9.234	7.016
51	8.89	3.14	15.828	14.125	14.25	15.328	13.516
52	10.8	3.14	25.531	21.125	21.359	22.734	21.719
53	12.7	3.14	36.937	0.016	0.016	0.016	0.016
54	14.61	3.14	0	0	0	45.937	0
55	4.13	3.53	2.531	3.234	2.422	3.531	1.922
56	6.03	3.53	6.437	6.437	5.734	6.937	5.125
57	7.94	3.53	11.937	11.531	10.859	11.937	9.922
58	9.84	3.53	19.734	17.937	17.75	18.828	17.016
59	11.75	3.53	30.141	26.625	25.953	28.437	26.516
60	13.65	3.53	42.547	38.531	36.359	40.937	40.516
61	5.08	3.93	3.734	4.437	3.531	4.937	3.219
62	6.99	3.93	8.328	8.328	7.453	8.937	7.016
63	8.89	3.93	15.125	13.937	13.156	15.031	13.328
64	10.8	3.93	23.734	21.234	20.562	23.141	21.219
65	12.7	3.93	34.937	31.125	30.453	33.531	33.125
66	14.61	3.93	0	0.016	0.016	0.016	0
67	4.13	4.32	1.922	2.734	1.922	3.328	1.625
68	6.03	4.32	5.437	5.734	0.016	0.016	4.516

Sensor #	Radial Distance(cm)	Radial line angle (radian)	Flow arrival time Experiment 1 (s)	Flow arrival time Experiment 2 (s)	Flow arrival time Experiment 3 (s)	Flow arrival time Experiment 4 (s)	Flow arrival time Experiment 5 (s)
69	7.94	4.32	11.125	10.437	9.75	11.437	9.422
70	9.84	4.32	18.437	16.625	16.25	18.141	15.719
71	11.75	4.32	27.937	24.828	25.359	27.031	25.719
72	13.65	4.32	41.047	37.328	36.656	39.734	40.125
73	5.08	4.71	3.531	3.937	3.234	4.828	2.625
74	6.99	4.71	7.437	7.234	6.734	8.531	6.125
75	8.89	4.71	13.531	12.437	11.953	14.328	11.328
76	10.8	4.71	22.031	19.437	19.359	22.531	18.922
77	12.7	4.71	32.531	28.031	28.156	32.641	29.328
78	14.61	4.71	46.844	41.125	39.578	45.734	42.922
79	4.13	5.11	2.031	2.828	2.016	3.328	1.625
80	6.03	5.11	5.625	5.625	4.937	6.641	4.219
81	7.94	5.11	10.734	10.031	9.562	11.328	8.516
82	9.84	5.11	18.031	15.625	15.75	17.828	14.922
83	11.75	5.11	27.828	23.531	24.656	26.641	24.422
84	13.65	5.11	40.641	34.437	34.359	0.016	37.516
85	5.08	5.5	3.625	4.328	0.016	0.016	2.922
86	6.99	5.5	8.125	7.937	7.141	8.937	6.516
87	8.89	5.5	15.125	13.234	12.953	15.234	12.922
88	10.8	5.5	23.625	20.125	0.016	0.016	0.016
89	12.7	5.5	35.141	29.234	29.859	34.828	32.625
90	14.61	5.5	49.937	43.437	41.875	0	0
91	4.13	5.89	2.328	3.234	2.219	3.625	1.922
92	6.03	5.89	6.031	0.016	0.016	0.016	0.016
93	7.94	5.89	11.937	11.234	10.453	12.734	10.422
94	9.84	5.89	19.125	17.125	16.859	20.141	17.625
95	11.75	5.89	28.625	25.625	25.156	30.141	28.422
96	13.65	5.89	43.547	39.437	36.766	44.328	43.625
97	0	0	0.016	0.828	0.016	1.031	0.016
98	4.13	0	2.125	3.125	2.219	3.531	1.922
99	6.03	0	0	0	0	0	0
100	7.94	0	11.031	10.937	10.359	12.141	10.219
101	9.84	0	18.531	17.734	17.156	19.437	18.219
102	11.75	0	29.031	25.734	25.562	28.531	29.125
103	13.65	0	44.047	39.734	37.062	42.531	43.219

104	4.13	0.39	2.328	3.234	2.219	3.531	2.016
105	6.03	0.39	5.828	6.437	5.531	6.734	5.328
Sensor #	**Radial Distance(cm)**	**Radial line angle (radian)**	**Flow arrival time Experiment 1 (s)**	**Flow arrival time Experiment 2 (s)**	**Flow arrival time Experiment 3 (s)**	**Flow arrival time Experiment 4 (s)**	**Flow arrival time Experiment 5 (s)**
106	7.94	0.39	11.437	11.234	10.656	11.437	10.219
107	9.84	0.39	19.234	18.234	17.562	18.234	18.016
108	11.75	0.39	30.031	27.031	26.062	28.141	27.719
109	13.65	0.39	43.844	40.437	36.766	40.437	42.125
110	4.13	0.79	2.125	3.125	2.219	3.328	2.016
111	6.03	0.79	5.828	6.437	5.641	6.437	5.516
112	7.94	0.79	11.437	11.437	10.562	11.531	10.828
113	9.84	0.79	19.125	17.937	16.75	17.641	18.625
114	11.75	0.79	29.437	26.625	24.859	26.234	29.016
115	4.13	1.18	2.125	3.031	2.219	3.328	1.922
116	6.03	1.18	5.531	6.031	5.437	6.437	5.125
117	7.94	1.18	11.031	10.828	10.453	11.141	10.422
118	9.84	1.18	18.937	17.437	17.062	18.031	17.922
119	11.75	1.18	29.531	25.531	25.359	26.531	28.328
120	13.65	1.18	18.937	38.828	15.953	38.031	42.922
121	4.13	1.57	2.234	2.922	2.219	3.328	1.922
122	6.03	1.57	5.937	6.125	5.641	6.531	5.328
123	7.94	1.57	11.125	10.625	10.25	11.234	10.328
124	9.84	1.57	18.531	17.125	17.062	18.031	17.422
125	11.75	1.57	28.328	24.937	25.359	27.328	9.828
126	13.65	1.57	41.734	38.031	36.156	39.734	42.125
127	4.13	1.96	2.234	3.125	2.328	3.437	2.016
128	6.03	1.96	5.625	6.234	5.437	6.641	4.922
129	7.94	1.96	11.328	10.734	10.359	11.328	9.719
130	9.84	1.96	19.437	17.125	17.359	18.437	17.219
131	11.75	1.96	28.734	25.031	25.359	27.437	9.828
132	13.65	1.96	43.641	38.234	36.859	40.031	0
133	4.13	2.36	2.234	3.234	2.328	3.437	1.922
134	6.03	2.36	6.031	6.328	5.437	6.828	5.016
135	7.94	2.36	11.734	10.937	10.656	11.734	9.719
136	9.84	2.36	19.125	17.234	17.25	18.328	16.719
137	11.75	2.36	29.531	25.734	26.359	27.234	26.625

138	13.65	2.36	43.437	37.937	37.672	38.937	40.719
139	4.13	2.75	2.328	3.125	2.328	3.531	1.922
Sensor #	**Radial Distance(cm)**	**Radial line angle (radian)**	**Flow arrival time Experiment 1 (s)**	**Flow arrival time Experiment 2 (s)**	**Flow arrival time Experiment 3 (s)**	**Flow arrival time Experiment 4 (s)**	**Flow arrival time Experiment 5 (s)**
140	6.03	2.75	6.328	6.437	5.641	6.937	5.125
141	7.94	2.75	19.734	0.016	0.016	0.016	0.016
142	9.84	2.75	19.734	0.016	0.016	0.016	0.016
143	11.75	2.75	30.937	0.016	0.016	0.016	26.328
144	13.65	2.75	44.844	39.328	37.172	41.328	39.516
145	4.13	3.14	2.422	3.234	2.328	3.531	1.828
146	6.03	3.14	6.625	0.016	5.734	7.141	5.016
147	7.94	3.14	12.125	11.328	10.953	12.141	9.922
148	9.84	3.14	21.328	18.125	18.062	19.234	17.625
149	11.75	3.14	31.328	26.328	26.359	27.937	27.516
150	13.65	3.14	45.734	40.437	37.969	40.031	41.328
151	4.13	3.53	2.531	3.234	2.422	3.531	1.828
152	6.03	3.53	6.437	6.531	5.844	7.031	5.125
153	7.94	3.53	12.328	11.437	11.156	12.031	10.328
154	9.84	3.53	20.234	18.234	17.953	19.437	17.516
155	11.75	3.53	30.328	27.531	26.656	28.828	27.625
156	13.65	3.53	44.141	40.328	37.359	42.531	42.016
157	4.13	3.93	2.328	3.031	2.125	3.625	1.922
158	6.03	3.93	6.031	6.125	5.437	6.937	4.922
159	7.94	3.93	11.531	11.125	10.359	11.828	9.922
160	9.84	3.93	19.531	17.734	16.859	18.734	17.625
161	11.75	3.93	0.016	26.437	25.656	28.531	27.828
162	13.65	3.93	43.234	38.828	37.266	41.828	41.219
163	4.13	4.32	2.031	2.625	1.922	3.328	1.516
164	6.03	4.32	5.531	5.734	5.031	6.641	4.625
165	7.94	4.32	18.625	17.031	16.359	18.437	16.328
166	9.84	4.32	18.625	17.031	16.359	18.437	16.328
167	11.75	4.32	28.234	25.734	25.359	27.734	26.016
168	13.65	4.32	28.234	25.734	25.359	27.734	26.016
169	4.13	4.71	2.031	0.016	0.016	0.016	0.016
170	6.03	4.71	5.437	5.328	4.828	6.437	4.219
171	7.94	4.71	10.125	9.437	9.562	11.328	8.625

172	9.84	4.71	17.531	16.031	15.75	18.437	15.016
173	11.75	4.71	27.625	23.734	23.953	27.937	24.719
Sensor #	**Radial Distance(cm)**	**Radial line angle (radian)**	**Flow arrival time Experiment 1 (s)**	**Flow arrival time Experiment 2 (s)**	**Flow arrival time Experiment 3 (s)**	**Flow arrival time Experiment 4 (s)**	**Flow arrival time Experiment 5 (s)**
174	13.65	4.71	42.344	35.734	34.75	40.031	37.516
175	4.13	5.11	2.031	2.734	2.016	3.328	1.516
176	6.03	5.11	5.437	5.625	4.937	6.531	4.219
177	7.94	5.11	10.828	9.937	9.562	11.141	8.422
178	9.84	5.11	18.328	15.828	15.953	17.937	15.219
179	11.75	5.11	27.734	23.734	24.359	27.641	24.625
180	13.65	5.11	41.734	34.937	34.453	39.234	38.516
181	4.13	5.5	2.031	3.031	2.125	3.437	1.625
182	6.03	5.5	5.625	5.828	5.234	6.641	4.516
183	7.94	5.5	10.828	10.437	9.859	12.141	9.516
184	9.84	5.5	18.937	16.328	16.656	19.437	16.922
185	11.75	5.5	29.328	24.625	25.156	29.531	27.016
186	13.65	5.5	43.641	36.125	36.062	42.437	40.922
187	4.13	5.89	2.031	2.922	2.016	3.437	1.719
188	6.03	5.89	6.125	6.234	5.437	7.234	5.219
189	7.94	5.89	0	0	0	0	
190	9.84	5.89	19.125	17.234	16.75	20.328	17.625
191	11.75	5.89	0	0	0	0	0
192	13.65	5.89	28.828	25.734	25.359	30.437	27.719

ELSEVIER LICENSE
TERMS AND CONDITIONS

Aug 20, 2010

This is a License Agreement between KENNETH OKONKWO ("You") and Elsevier ("Elsevier") provided by Copyright Clearance Center ("CCC"). The license consists of your order details, the terms and conditions provided by Elsevier, and the payment terms and conditions.

All payments must be made in full to CCC. For payment instructions, please see information listed at the bottom of this form.

Supplier	Elsevier Limited The Boulevard,Langford Lane Kidlington,Oxford,OX5 1GB,UK
Registered Company Number	1982084
Customer name	KENNETH OKONKWO
Customer address	126 SPENCER LAB
	NEWARK, DE 19716
License number	2493281124027
License date	Aug 20, 2010
Licensed content publisher	Elsevier
Licensed content publication	Composites Part A: Applied Science and Manufacturing
Licensed content title	Asymptotic expansion homogenization of permeability tensor for plain woven fabrics
Licensed content author	Y.S. Song, J.R. Youn
Licensed content date	November 2006
Licensed content volume number	37
Licensed content issue number	11
Number of pages	8
Type of Use	reuse in a thesis/dissertation
Requestor type	Not specified
Intended publisher of new work	n/a
Portion	figures/tables/illustrations
Number of figures/tables /illustrations	1
Format	both print and electronic
Are you the author of this Elsevier article?	No
Will you be translating?	No
Order reference number	

Title of your thesis/dissertation	3D PERMEABILITY CHARACTERIZATION OF FIBROUS MEDIA
Expected completion date	Aug 2010
Estimated size (number of pages)	100
Elsevier VAT number	GB 494 6272 12
Terms and Conditions	

INTRODUCTION

1. The publisher for this copyrighted material is Elsevier. By clicking "accept" in connection with completing this licensing transaction, you agree that the following terms and conditions apply to this transaction (along with the Billing and Payment terms and conditions established by Copyright Clearance Center, Inc. ("CCC"), at the time that you opened your Rightslink account and that are available at any time at http://myaccount.copyright.com).

GENERAL TERMS

2. Elsevier hereby grants you permission to reproduce the aforementioned material subject to the terms and conditions indicated.

3. Acknowledgement: If any part of the material to be used (for example, figures) has appeared in our publication with credit or acknowledgement to another source, permission must also be sought from that source. If such permission is not obtained then that material may not be included in your publication/copies. Suitable acknowledgement to the source must be made, either as a footnote or in a reference list at the end of your publication, as follows:

"Reprinted from Publication title, Vol /edition number, Author(s), Title of article / title of chapter, Pages No., Copyright (Year), with permission from Elsevier [OR APPLICABLE SOCIETY COPYRIGHT OWNER]." Also Lancet special credit - "Reprinted from The Lancet, Vol. number, Author(s), Title of article, Pages No., Copyright (Year), with permission from Elsevier."

4. Reproduction of this material is confined to the purpose and/or media for which permission is hereby given.

5. Altering/Modifying Material: Not Permitted. However figures and illustrations may be altered/adapted minimally to serve your work. Any other abbreviations, additions, deletions and/or any other alterations shall be made only with prior written authorization of Elsevier Ltd. (Please contact Elsevier at permissions@elsevier.com)

6. If the permission fee for the requested use of our material is waived in this instance, please be advised that your future requests for Elsevier materials may attract a fee.

7. Reservation of Rights: Publisher reserves all rights not specifically granted in the combination of (i) the license details provided by you and accepted in the course of this licensing transaction, (ii) these terms and conditions and (iii) CCC's Billing and

Payment terms and conditions.

8. License Contingent Upon Payment: While you may exercise the rights licensed immediately upon issuance of the license at the end of the licensing process for the transaction, provided that you have disclosed complete and accurate details of your proposed use, no license is finally effective unless and until full payment is received from you (either by publisher or by CCC) as provided in CCC's Billing and Payment terms and conditions. If full payment is not received on a timely basis, then any license preliminarily granted shall be deemed automatically revoked and shall be void as if never granted. Further, in the event that you breach any of these terms and conditions or any of CCC's Billing and Payment terms and conditions, the license is automatically revoked and shall be void as if never granted. Use of materials as described in a revoked license, as well as any use of the materials beyond the scope of an unrevoked license, may constitute copyright infringement and publisher reserves the right to take any and all action to protect its copyright in the materials.

9. Warranties: Publisher makes no representations or warranties with respect to the licensed material.

10. Indemnity: You hereby indemnify and agree to hold harmless publisher and CCC, and their respective officers, directors, employees and agents, from and against any and all claims arising out of your use of the licensed material other than as specifically authorized pursuant to this license.

11. No Transfer of License: This license is personal to you and may not be sublicensed, assigned, or transferred by you to any other person without publisher's written permission.

12. No Amendment Except in Writing: This license may not be amended except in a writing signed by both parties (or, in the case of publisher, by CCC on publisher's behalf).

13. Objection to Contrary Terms: Publisher hereby objects to any terms contained in any purchase order, acknowledgment, check endorsement or other writing prepared by you, which terms are inconsistent with these terms and conditions or CCC's Billing and Payment terms and conditions. These terms and conditions, together with CCC's Billing and Payment terms and conditions (which are incorporated herein), comprise the entire agreement between you and publisher (and CCC) concerning this licensing transaction. In the event of any conflict between your obligations established by these terms and conditions and those established by CCC's Billing and Payment terms and conditions, these terms and conditions shall control.

14. Revocation: Elsevier or Copyright Clearance Center may deny the permissions described in this License at their sole discretion, for any reason or no reason, with a full refund payable to you. Notice of such denial will be made using the contact information provided by you. Failure to receive such notice will not alter or invalidate the denial. In no event will Elsevier or Copyright Clearance Center be responsible or liable for any costs, expenses or damage incurred by you as a result of a denial of your permission request, other than a refund of the amount(s) paid

by you to Elsevier and/or Copyright Clearance Center for denied permissions.

LIMITED LICENSE

The following terms and conditions apply only to specific license types:

15. **Translation**: This permission is granted for non-exclusive world **English** rights only unless your license was granted for translation rights. If you licensed translation rights you may only translate this content into the languages you requested. A professional translator must perform all translations and reproduce the content word for word preserving the integrity of the article. If this license is to re-use 1 or 2 figures then permission is granted for non-exclusive world rights in all languages.

16. **Website**: The following terms and conditions apply to electronic reserve and author websites:
Electronic reserve: If licensed material is to be posted to website, the web site is to be password-protected and made available only to bona fide students registered on a relevant course if:
This license was made in connection with a course,
This permission is granted for 1 year only. You may obtain a license for future website posting,
All content posted to the web site must maintain the copyright information line on the bottom of each image,
A hyper-text must be included to the Homepage of the journal from which you are licensing at http://www.sciencedirect.com/science/journal/xxxxx or the Elsevier homepage for books at http://www.elsevier.com , and
Central Storage: This license does not include permission for a scanned version of the material to be stored in a central repository such as that provided by Heron/XanEdu.

17. **Author website** for journals with the following additional clauses:

All content posted to the web site must maintain the copyright information line on the bottom of each image, and
he permission granted is limited to the personal version of your paper. You are not allowed to download and post the published electronic version of your article (whether PDF or HTML, proof or final version), nor may you scan the printed edition to create an electronic version,
A hyper-text must be included to the Homepage of the journal from which you are licensing at http://www.sciencedirect.com/science/journal/xxxxx , As part of our normal production process, you will receive an e-mail notice when your article appears on Elsevier's online service ScienceDirect (www.sciencedirect.com). That e-mail will include the article's Digital Object Identifier (DOI). This number provides the electronic link to the published article and should be included in the posting of your personal version. We ask that you wait until you receive this e-mail and have the DOI to do any posting.
Central Storage: This license does not include permission for a scanned version of the material to be stored in a central repository such as that provided by Heron/XanEdu.

18. **Author website** for books with the following additional clauses:
Authors are permitted to place a brief summary of their work online only.
A hyper-text must be included to the Elsevier homepage at
http://www.elsevier.com

All content posted to the web site must maintain the copyright information line on the bottom of each image
You are not allowed to download and post the published electronic version of your chapter, nor may you scan the printed edition to create an electronic version.
Central Storage: This license does not include permission for a scanned version of the material to be stored in a central repository such as that provided by Heron/XanEdu.

19. **Website** (regular and for author): A hyper-text must be included to the Homepage of the journal from which you are licensing at http://www.sciencedirect.com/science/journal/xxxxx. or for books to the Elsevier homepage at http://www.elsevier.com

20. **Thesis/Dissertation**: If your license is for use in a thesis/dissertation your thesis may be submitted to your institution in either print or electronic form. Should your thesis be published commercially, please reapply for permission. These requirements include permission for the Library and Archives of Canada to supply single copies, on demand, of the complete thesis and include permission for UMI to supply single copies, on demand, of the complete thesis. Should your thesis be published commercially, please reapply for permission.

21. **Other Conditions**:

v1.6

Gratis licenses (referencing $0 in the Total field) are free. Please retain this printable license for your reference. No payment is required.

If you would like to pay for this license now, please remit this license along with your payment made payable to "COPYRIGHT CLEARANCE CENTER" otherwise you will be invoiced within 48 hours of the license date. Payment should be in the form of a check or money order referencing your account number and this invoice number RLNK10835432.
Once you receive your invoice for this order, you may pay your invoice by credit card. Please follow instructions provided at that time.

Make Payment To:
Copyright Clearance Center
Dept 001
P.O. Box 843006
Boston, MA 02284-3006

If you find copyrighted material related to this license will not be used and wish to cancel, please contact us referencing this license number 2493281124027 and noting the reason for cancellation.

Questions? customercare@copyright.com or +1-877-622-5543 (toll free in the US) or +1-978-646-2777.